PPPL-2331

25

PPPL-2331

UC20-G

PPPL--2331

DE86 011370

ANALYTIC GRAD-SHAFRANOV TEST CRITERIA AND CHECKS OF A 1-1/2-D BALDUR TRANSPORT CODE

By

F.G.P. Seidl

MAY 1986

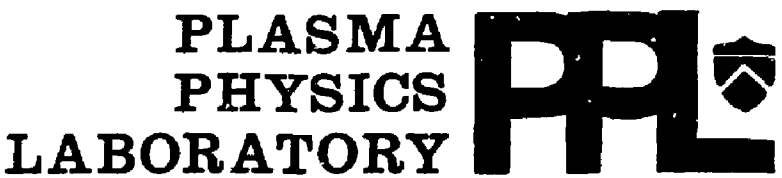

PRINCETON UNIVERSITY

PRINCETON, NEW JERSEY

PREPARED FOR THE U.S. DEPARTMENT OF ENERGY,
UNDER CONTRACT DE-AC02-76-CHO-3073.

EXTERNAL DISTRIBUTION IN ADDITION TO UC-20

Plasma Res Lab, Austra Nat'l Univ, AUSTRALIA
Dr. Frank J. Paoloni, Univ of Wollongong, AUSTRALIA
Prof. I.R. Jones, Flinders Univ., AUSTRALIA
Prof. M.H. Brennan, Univ Sydney, AUSTRALIA
Prof. F. Cap, Inst Theo Phys, AUSTRIA
M. Goossens, Astronomisch Instituut, BELGIUM
Prof. R. Boucique, Laboratorium voor Natuurkunde, BELGIUM
Dr. D. Palumbo, Dg XII Fusion Prog, BELGIUM
Ecole Royale Militaire, Lab de Phys Plasmas, BELGIUM
Dr. P.H. Sakanaka, Univ Estadual, BRAZIL
Lib. & Doc. Div., Instituto de Pesquisas Espaciais, BRAZIL
Dr. C.R. James, Univ of Alberta, CANADA
Prof. J. Teichmann, Univ of Montreal, CANADA
Dr. H.M. Skarsgard, Univ of Saskatchewan, CANADA
Prof. S.R. Sreenivasan, University of Calgary, CANADA
Prof. Tudor W. Johnston, INRS-Energie, CANADA
Dr. Hannes Barnard, Univ British Columbia, CANADA
Dr. M.P. Bachynski, MPB Technologies, Inc., CANADA
Chalk River, Nucl Lab, CANADA
Zhengwu Li, SK Inst Physics, CHINA
Library, Tsing Hua University, CHINA
Librarian, Institute of Physics, CHINA
Inst Plasma Phys, Academia Sinica, CHINA
Dr. Peter Lukac, Komenskeho Univ, CZECHOSLOVAKIA
The Librarian, Culham Laboratory, ENGLAND
Prof. Schatzman, Observatoire de Nice, FRANCE
J. Radet, CEN-BP6, FRANCE
JET Reading Room, JET Joint Undertaking, ENGLAND
AM Dupas Library, AM Dupas Library, FRANCE
Dr. Tom Mual, Academy Bibliographic, HONG KONG
Preprint Library, Cent Res Inst Phys, HUNGARY
Dr. R.K. Chhajlani, Vikram Univ, INDIA
Dr. B. Dasgupta, Saha Inst, INDIA
Dr. P. Kaw, Physical Research Lab, INDIA
Dr. Phillip Rosenau, Israel Inst Tech, ISRAEL
Prof. S. Cuperman, Tel Aviv University, ISRAEL
Prof. G. Rostagni, Univ Di Padova, ITALY
Librarian, Int'l Ctr Theo Phys, ITALY
Miss Clelia De Palo, Assoc EURATOM-ENEA, ITALY
Biblioteca, del CNR EURATOM, ITALY
Dr. H. Yamato, Toshiba Res & Dev, JAPAN
Direc. Dept. Lg. Tokamak Dev. JAERI, JAPAN
Prof. Nobuyuki Inoue, University of Tokyo, JAPAN
Research Info Center, Nagoya University, JAPAN
Prof. Kyoji Nishikawa, Univ of Hiroshima, JAPAN
Prof. Sigeru Mori, JAERI, JAPAN
Prof. S. Tanaka, Kyoto University, JAPAN
Library, Kyoto University, JAPAN
Prof. Ichiro Kawakami, Nihon Univ, JAPAN
Prof. Satoshi Itoh, Kyushu University, JAPAN
Dr. D.I. Choi, Adv. Inst Sci & Tech, KOREA
Tech Info Division, KAERI, KOREA
Bibliotheek, Fom-Inst Voor Plasma, NETHERLANDS
Prof. B.S. Liley, University of Waikato, NEW ZEALAND
Prof. J.A.C. Cabral, Inst Superior Tecn, PORTUGAL
Dr. Octavian Petrus, ALI CUZA University, ROMANIA
Prof. M.A. Hellberg, University of Natal, SO AFRICA
Dr. Johan de Villiers, Plasma Physics, Nucor, SO AFRICA
Fusion Div. Library, JEN, SPAIN
Prof. Hans Wilhelmson, Chalmers Univ Tech, SWEDEN
Dr. Lennart Stenflo, University of UMEA, SWEDEN
Library, Royal Inst Tech, SWEDEN
Centre de Recherchesen, Ecole Polytech Fed, SWITZERLAND
Dr. V.T. Tolok, Kharkov Phys Tech Ins, USSR
Dr. D.D. Ryutov, Siberian Acad Sci, USSR
Dr. G.A. Ellseev, Kurchatov Institute, USSR
Dr. V.A. Glukhikh, Inst Electro-Physical, USSR
Institute Gen. Physics, USSR
Prof. T.J.M. Boyd, Univ College N Wales, WALES
Dr. K. Schindler, Ruhr Universitat, W. GERMANY
ASDEX Reading Rm, IPP/Max-Planck-Institut fur Plasmaphysik, F.R.G.
Nuclear Res Estab, Julich Ltd, W. GERMANY
Librarian, Max-Planck Institut, W. GERMANY
Bibliothek, Inst Plasmaforschung, W. GERMANY
Prof. R.K. Janev, Inst Phys, YUGOSLAVIA

ANALYTIC GRAD-SHAFRANOV TEST CRITERIA AND CHECKS OF A 1-1/2-D BALDUR TRANSPORT CODE

F. G. P. Seidl

Plasma Physics Laboratory, Princeton University

Princeton, N.J. 08544

ABSTRACT

As discussed by Shafranov, Solov'ev, and others, two special constraints allow the Grad-Shafranov equation to yield simple analytic solutions. From the simplest solution, formulae are derived for properties of the corresponding toroidally symmetric plasma and for the space profile of poloidal magnetic flux density. These formulae constitute test criteria for code performance once the code is made consistent with the two constraints. Obtaining consistency with the first constraint is straightforward, but with the second it is circumstantial. Moreover, the poloidal flux profile of the analytic solution implies a certain artificial form for the resistivity, which is also derived. These criteria have been used to check a composite code which had been assembled by linking a geometrically generalized 1-D BALDUR transport code with a computationally efficient 2-D equilibrium code. A brief description of the composite code is given as well as of its performance with respect to the Grad-Shafranov test criteria.

CONTENTS

1. MOTIVATION

The Tokamak Modeling Group, under D. E. Post at Princeton Plasma Physics Laboratory, is involved in developing and using large computer codes which simulate on a resistive time scale many aspects of tokamak experiments. There are certainly four main areas of activity: (1) transport codes (e.g., BALDUR, see Refs. 1 and 2); (2) neutral gas transport (e.g., DEGAS, Ref. 3); (3) a divertor code (e.g., PLANET, Ref. 4); and, (4) impurity transport (e.g., MIST, Ref. 5). Moreover, work in the main areas is enhanced by beam penetration codes, an atomic physics data code, various simple divertor codes, beam orbit codes, etc. All this is part of the general effort to improve both the understanding of tokamak physics and the capability to predict future experimental results. The considerations described here have to do with contributing to the first category, i.e., transport code development.

As tokamak experiments evolve beyond exploiting toroidal plasmas of circularly symmetric cross sections, there is a need to model plasmas of noncircular cross sections, and perhaps, even to estimate effects which are poloidally asymmetric. Some movement in this direction has been made by linking an upgraded version of the BALDUR 1-D code with 2-D MHD equilibrium subprograms. The work reported here stems from recognizing the need to check performance accuracy of 2-D MHD subprograms as well as associated aspects of numerical simulations, for example, the calculation of poloidal magnetic flux density. More immediately, it was important to check the first 1-1/2-D extension of the BALDUR transport code.

2. OBJECTIVES

Our fundamental objectives have to do with modeling a toroidally symmetric plasma confined by a magnetic field, where the geometry of the

plasma is allowed to evolve in time and the minor cross section can be noncircular. We are interested in finding a way to test the numerical results against analytically determined values with the understanding that this is feasible only under limited conditions. As a starting point, it is recognized that the Grad-Shafranov equation yields analytic solutions when subject to certain constraints (Refs. 6 and 7), which will be referred to as the "Shafranov-Solov'ev constraints." In particular, the first of our objectives is to derive tractable formulae for the geometric properties of the simplest analytic solutions. The formulae (i.e., "test criteria") would then be available for checking the accuracy of certain code calculations and would include the Shafranov shift, elongation, triangularity, volume enclosed by constant-flux surface, etc. Initial applications would involve the first BALDUR-MHD 1-1/2-D transport code (Ref. 8), also described under Sec. 8A.

The second objective is to make the test criteria relevant by finding ways to match the Shafranov-Solev'ev constraints as closely as possible in the algorithms of the program under test. Obviously, limitations must be imposed on the choice of initial and boundary conditions for the numerical solution. But, in addition, it is realized that certain physical realities are often inconsistent with the implications of the constraints which allow analytic solutions. Some of the physical implications of these constraints are considered in Sec. 6 of this paper.

The third of our objectives is to examine the physical implications of the first Shafranov-Solov'ev constraint in order to derive one or more analytic formulae describing the spatial variation of the poloidal magnetic flux, and this should be feasible since poloidal flux is, of course, the principal dependent variable of the Grad-Shafranov equation. Having an exact formula for poloidal flux, or more precisely poloidal flux density χ', the

test procedure can be extended to include checking numerical calculations of χ'. Such calculations are normally carried out in the transport part of a composite code and depend on solving a nonlinear diffusion type equation. This kind of test is significant but, since diffusion-like equations for χ' inevitably involve plasma resistivity, a final objective is to discover just how the resistivity *must* be modified so as to become consistent with the physical implications of the Shafranov-Solov'ev constraints.

3. COORDINATE GEOMETRY

Consider the representation of an axially symmetric toroidal plasma. Local properties of the plasma can be described in terms of a fixed cylindrical orthogonal coordinate system

$$\vec{x} \equiv (R,Z,\phi) \ , \tag{3.1}$$

in which R denotes the major radius to a local point, Z the height of this point above a horizontal midplane, and ϕ is the toroidal angle where $0 \leq \phi \leq 2\pi$. The plasma is assumed to be confined by a magnetic field $\vec{B}$ under conditions of quasistationary pressure balance:

$$\vec{\nabla}P = \frac{1}{c}\left(\vec{J} \times \vec{B}\right) \ , \tag{3.2}$$

$$\vec{\nabla} \times \vec{B} = \frac{4\pi}{c}\vec{J} \ , \tag{3.3}$$

$$\vec{\nabla}\cdot\vec{B} = 0 \ , \tag{3.4}$$

where P denotes plasma pressure

$$P = P_e + \sum_a P_a + [\text{fast-ion effects which are neglected}], \tag{3.5}$$

and $\vec{J}$ is current density. When P is reasonably smooth, a set of constant-P surfaces can exist in the plasma; and, since from (3.2)

$$\vec{B}\cdot\vec{\nabla}P = 0 , \tag{3.6}$$

each of these surfaces is a magnetic surface (or flux surface) in the sense that it can be generated by the ergodic trace of a magnetic field line $\vec{B}$ [9] which does not close on itself within a finite number of turns. In view of toroidal symmetry and the conditions (3.2) through (3.4), it is assumed [10] that the flux surfaces form a family of nested toroids and that the innermost such surface degenerates into a curved line called the magnetic axis which does actually close on itself. Further remarks concerning the existence of magnetic surfaces can be found in Ref. 9. In the case of the analytic solutions subsequently described, it can be proven that there are embedded in these solutions families of nested toroids, each family converging onto a common magnetic axis, and each toroid corresponding to a surface of constant poloidal flux density.

Based on such nested flux surfaces, a flux-coordinate system can be set up in which the principal variable is taken to be a generalized minor radius ρ that, by definition, is constant for any flux surface, zero on the magnetic axis, and reaches its maximum value (max ρ = a) on what is taken to be the outermost flux surface. The domain of ρ is

$$\rho \in [0,a]. \tag{3.7}$$

Due to the one-to-one correspondence between an arbitrary value of ρ and a particular flux surface, ρ constitutes a flux-surface label. Since flux surfaces are also surfaces of constant pressure P,

$$\vec{\nabla}P = \frac{\partial P(\rho,t)}{\partial \rho}\,\vec{\nabla}\rho\ , \tag{3.8}$$

and, consequently, from Eq. (3.2)

$$\vec{B}\cdot\vec{\nabla}\rho = \vec{J}\cdot\vec{\nabla}\rho = 0. \tag{3.9}$$

The second variable in the flux-coordinate system is θ, which is allowed to increase from 0 to 2π along the shortest path around the flux surface ρ, and is made definite by prescribing the Jacobian $\sqrt{g}$ for the transformation from the fixed frame $\vec{x} = (R,Z,\phi)$ to the flux-coordinate frame (ρ,θ,ϕ), where the latter may be evolving with time. The toroidal angle ϕ is the same in both frames. Expressed in terms of the reciprocal basis vectors $\vec{\nabla}\rho$, $\vec{\nabla}\theta$, and $\vec{\nabla}\phi$, the Jacobian is given by

$$\sqrt{g} = \left[(\vec{\nabla}\rho \times \vec{\nabla}\theta)\cdot\vec{\nabla}\phi\right]^{-1}$$

$$= R\left(R_\theta Z_\rho - R_\rho Z_\theta\right). \tag{3.10}$$

The requirement that ρ be constant over a particular (generally noncircular) flux surface while θ varies from 0 to 2π in a convenient way can prevent $\vec{\nabla}\rho$ and $\vec{\nabla}\theta$ from being orthogonal. Relationships between reciprocal basis vectors

thus become

$$\vec{\nabla}\rho\cdot\vec{\nabla}\theta \neq 0 \ , \tag{3.11}$$

$$\vec{\nabla}\theta\cdot\vec{\nabla}\phi = 0 \ , \tag{3.12}$$

$$\vec{\nabla}\phi\cdot\vec{\nabla}\rho = 0 \ , \tag{3.13}$$

and also

$$\vec{\nabla}\phi\cdot\vec{\nabla}\phi = R^{-2} \ , \tag{3.14}$$

where R is the local major radius. Equations (3.11) through (3.14) constitute basic properties of the flux-coordinate geometry.

By treating the principal flux-coordinate ρ as a parameter, equations in (R,Z,ϕ) space for constant-flux surfaces (i.e., constant-ρ surfaces) can be expressed as Fourier series (e.g., Ref. 11):

$$R(\rho,\theta,t) = \sum_n R_n(\rho,t) \ \cos(n\theta), \tag{3.15}$$

and

$$Z(\rho,\theta,t) = \sum_n Z_n(\rho,t) \ \sin(n\theta), \tag{3.16}$$

where R and Z have units of length. Other forms for the principal flux coordinate can, of course, be reinterpreted in terms of ρ, which here is taken to be the plasma minor radius on the horizontal midplane; e.g.,

$$\rho \equiv \frac{1}{2}\sum_n R_n(\phi,t) \ [1 - \cos(nr)], \tag{3.17}$$

where Φ represents toroidal flux.

The physical effects to be represented in terms of flux coordinates evolve on the resistive time scale [12-14] in terms of which certain interesting properties (e.g., particle densities and ion temperatures) approach uniformity over a flux surface [13-15]. Consequently, meaningful results remain after the poloidal coordinate θ is eliminated by flux-surface averaging, which for an arbitrary scalar function F can be defined by the operation

$$\langle F \rangle_f \equiv \frac{\int_0^{2\pi} F \sqrt{g}\, d\theta}{\int_0^{2\pi} \sqrt{g}\, d\theta} \quad , \tag{3.18}$$

while the area of a toroidal flux surface ρ is given by

$$\text{flux-surface area} = V'(\rho,t) \langle |\vec{\nabla}\rho| \rangle_f \quad , \tag{3.19}$$

where

$$V'(\rho,t) = 2\pi \int_0^{2\pi} \sqrt{g}\ d\theta \quad , \tag{3.20}$$

and where the total volume enclosed by the flux surface is

$$V(\rho,t) = \int_0^{\rho} V'(\rho,t)\, d\rho. \tag{3.21}$$

To demonstrate the consistency of (3.19), note that an area element of a constant-ρ surface in a nonorthogonal space is, in general, given by $d\vec{A}^{(1)} = \vec{\nabla}\rho\ \sqrt{g}\ d\theta\ d\phi$, where $\sqrt{g}$ denotes the Jacobian. Evidently, the total surface area $S(\rho,t)$ is the accumulation of these surface elements:

$$S(\rho,t) = \int_{\phi=0}^{2\pi} \int_{\theta=0}^{2\pi} |\vec{\nabla}\rho| \sqrt{g}\, d\theta\, d\phi$$

$$= \frac{\int_0^{2\pi} |\vec{\nabla}\rho| \sqrt{g}\, d\theta}{\int_0^{2\pi} \sqrt{g}\, d\theta} \, 2\pi \int_0^{2\pi} \sqrt{g}\, d\theta$$

$$= \langle |\vec{\nabla}\rho| \rangle_f \, V'(\rho,t). \tag{3.22}$$

For purposes of representing in flux coordinates the equations for the cross-field transport of flux-surface-averaged quantities, extensive use is made of the following general theorem which expresses the flux-surface average of the divergence of an arbitrary vector function $\vec{A}$

$$\langle \vec{\nabla}\cdot\vec{A} \rangle_f = \frac{1}{V'} \frac{\partial}{\partial\rho} \left[V' \langle \vec{A}\cdot\vec{\nabla}\rho \rangle_f \right]. \tag{3.23}$$

Note, if it is assumed that as ρ approaches zero the toroidal flux surface corresponding to ρ collapses onto a closed loop (the magnetic axis), and if the coordinate ρ is expressed in units of length, then it follows that the Jacobian $\sqrt{g}$ must satisfy the condition

$$\lim_{\rho\to 0} \left(\frac{1}{2\pi} \int_0^{2\pi} \sqrt{g}\, d\theta \right) = 0. \tag{3.24}$$

Finally, for easy reference, two metric quantities are set out below. These are useful in reducing relations involving toroidal flux and poloidal flux, respectively

$$G_\phi(\rho,t) \equiv \frac{1}{2\pi} \int_0^{2\pi} \frac{1}{R^2} \sqrt{g}\, d\theta \ , \tag{3.25}$$

$$G_\theta(\rho,t) \equiv \frac{1}{2\pi}\int_0^{2\pi} \frac{(\vec{\nabla}\rho)^2}{R^2}\sqrt{g}\, d\theta \ . \tag{3.26}$$

4. THE EQUILIBRIUM EQUATION (GRAD-SHAFRANOV) FOR POLOIDAL FLUX AND CONSTRAINTS WHICH YIELD ANALYTIC SOLUTIONS

The Grad-Shafranov equilibrium equation for poloidal flux $\chi(\rho)$ follows directly from the pressure balance equation (3.2) once general expressions for $\vec{B}$ and $\vec{J}$ are introduced. In terms of flux coordinates (ρ,θ,ϕ) the contravariant expression for the total magnetic field $\vec{B}$ in an environment where $\vec{\nabla}\cdot\vec{B} = 0$ can be written as

$$\vec{B} = \frac{1}{2\pi}\chi'(\rho,t)\,(\vec{\nabla}\phi \times \vec{\nabla}\rho) + g(\rho,t)\,\vec{\nabla}\phi \ , \tag{4.1}$$

where by Eq. (3.9) $\vec{B}\cdot\vec{\nabla}\rho = 0$ and where

$$\chi'(\rho,t) \equiv 2\pi\,(\vec{B}\cdot\vec{\nabla}\theta)\,\sqrt{g} \tag{4.2}$$

is the poloidal flux density and

$$g(\rho,t) \equiv R^2(\vec{B}\cdot\vec{\nabla}\phi) \tag{4.3}$$

is the toroidal flux function, while $\sqrt{g}$ denotes the Jacobian [see Eq. (3.10)]. Note that a fundamental definition of poloidal flux $\chi(\rho,t)$ is given by

$$\chi(\rho,t) = \int_{\rho=0}^{\rho}\int_{\phi=0}^{2\pi} (\vec{B}\cdot\vec{\nabla}\theta)\,\sqrt{g}\, d\phi\, d\rho, \tag{4.4}$$

which corresponds to

$$\chi(\rho,t) = \int_{\rho=0}^{\rho} \chi'(\rho,t)\, d\rho \ , \tag{4.5}$$

where in the case of axisymmetric systems $\chi'(\rho,t)$ is defined by Eq. (4.2). Due to Eq. (3.4), $\chi'(\rho,t)$ is independent of θ; i.e., $\chi'(\rho,t)$ is a surface function. Moreover, the useful relations set out immediately below can be inferred from Ampere's law [i.e., Eq. (3.3)] and the tensor formula for the curl:

$$\vec{J}\cdot\vec{\nabla}\rho = + \frac{c}{4\pi} \frac{1}{\sqrt{g}} \frac{\partial}{\partial\theta}\, g(\rho,t) \ , \tag{4.6}$$

$$\vec{J}\cdot\vec{\nabla}\theta = - \frac{c}{4\pi} \frac{1}{\sqrt{g}} \frac{\partial}{\partial\rho}\, g(\rho,t) \ , \tag{4.7}$$

and, with the help of Eqs. (3.12) and (3.14) as well as certain vector identities,

$$\vec{J}\cdot\vec{\nabla}\phi = \frac{c}{8\pi^2}\, \vec{\nabla}\cdot\left(\frac{1}{R^2}\, \chi'(\rho,t)\, \vec{\nabla}\rho\right). \tag{4.8}$$

According to (3.9), (4.6) must vanish, showing that $g(\rho,t)$ is a surface function. Equations (4.7) and (4.8) complement the following contravariant formula for current density:

$$\vec{J} = \left(\vec{J}\cdot\vec{\nabla}\theta\right) \sqrt{g}\, \left(\vec{\nabla}\phi \times \vec{\nabla}\rho\right) + \left(\vec{J}\cdot\vec{\nabla}\phi\right) \sqrt{g}\, \left(\vec{\nabla}\rho \times \vec{\nabla}\theta\right). \tag{4.9}$$

The substitution of (4.1) for $\vec{B}$ and (4.9) for $\vec{J}$ into (3.2), combined with the use of (3.8) and (3.11) through (3.14), yields the Grad-Shafranov equation (Ampere's law giving $\vec{J}\cdot\vec{\nabla}\theta$ and $\vec{J}\cdot\vec{\nabla}\phi$)

$$\Delta^* \chi(\rho,t) + \frac{(2\pi)^2}{\chi(\rho,t)} \left(4\pi R^2 \frac{\partial P(\rho,t)}{\partial \rho} + g(\rho,t) \frac{\partial g(\rho,t)}{\partial \rho}\right) = 0, \tag{4.10}$$

where for an arbitrary scaler function F

$$\Delta^* F \equiv R^2 \vec{\nabla} \cdot \left[R^{-2} \vec{\nabla} F\right]. \tag{4.11}$$

On reverting to the fixed coordinates (R,Z,ϕ), Eq. (4.10) becomes

$$\frac{\partial^2 \chi}{\partial R^2} - \frac{1}{R} \frac{\partial \chi}{\partial R} + \frac{\partial^2 \chi}{\partial Z^2} = - \frac{8\pi^2}{c} \left[A(\chi) R^2 + B(\chi)\right], \tag{4.12}$$

[e.g., see Eq. (4.18), p. 116, Ref. 6] where

$$A(\chi) \equiv 2\pi c \frac{\partial P}{\partial \chi} = \frac{2\pi c}{\chi(\rho,t)} \frac{\partial P(\rho,t)}{\partial \rho}, \tag{4.13}$$

and

$$B(\chi) \equiv \frac{c}{2} g(\chi,t) \frac{\partial g(\chi,t)}{\partial \chi} = \frac{c}{2} \frac{g(\rho,t)}{\chi(\rho,t)} \frac{\partial g(\rho,t)}{\partial \rho}. \tag{4.14}$$

As pointed out on p. 116 of Ref. 6 and also on p. 402 of Ref. 7, the simplest family of analytic solutions of (4.12) becomes available by imposing the constraints

$$A(\chi) \equiv -A_o = \text{constant}, \tag{4.15}$$

and

$$B(\chi) \equiv 0. \tag{4.16}$$

Incidentally, while it is often true in the case of tokamak plasmas that $|B(\chi)| << |A(\chi)|R^2$, it is not necessarily correct from the physics standpoint

to neglect $B(\chi)$. As described in Ref. 7, a hierarchy of analytic solutions is actually available by assigning nontrivial values to $B(\chi)$. Since all these solutions are somewhat nonphysical anyway, only the simplest type is worked with here.

Under the constraints (4.15) and (4.16), Eq. (4.12) reduces to

$$\frac{\partial^2\chi}{\partial R^2} - \frac{1}{R}\frac{\partial\chi}{\partial R} + \frac{\partial^2\chi}{\partial Z^2} = +\frac{8\pi^2}{c} A_o R^2 , \tag{4.17}$$

which yields particular solutions corresponding to constant-χ surfaces of the form

$$\chi(\rho) = \chi(R,Z) = \psi_o \frac{(R_m^2 - R^2)^2 + 4\,\alpha^2 Z^2 R^2}{R_m^4} , \tag{4.18}$$

where R_m is the major radius out to the point $R = R_m$, $Z = 0$, namely out to the magnetic axis. The parameters R_m, α^2, and ψ_o are constants which can be chosen to approach realistic conditions; e.g., R_m can be set equal to the major radius out to the magnetic axis. Substitution of (4.18) into (4.17) shows that

$$A_o = \frac{c}{\pi^2}\frac{1+\alpha^2}{R_m^4}\psi_o . \tag{4.19}$$

Moreover, the form of (4.18) has, for convenience, been chosen so that

$$\lim_{\rho\to o} \chi(\rho) = \chi(R_m,0) = 0. \tag{4.20}$$

In actual toroidal plasmas, the poloidal field, $B_p = \chi(\rho,t)|\vec{\nabla}\rho|/(2\pi R)$, maintains its direction over the region $0 \le \rho \le a$, assuming that X-points and

such only occur where $\rho > a$. Consequently, it is reasonable to assume that

$$\chi'(\rho,t) \geq 0 \quad \text{for } \rho \in (0,a] \ , \tag{4.21}$$

which because of (4.5) implies that due to physical reasons

$$0 \leq \chi(\rho - |\Delta\rho|) \leq \chi(\rho) \leq \chi(a) \quad \text{for } \rho \in [|\Delta\rho|,a] \ ; \tag{4.22}$$

and, this condition supports the view that in physical reality $\lambda(\rho) \equiv \chi(\rho)/\psi_o$ is a monotonic increasing function of ρ.

The association of R_m in Eq. (4.18) with the magnetic axis is almost immediately obvious, while the significance of a^2 and ψ_o is worked out in the following sections dealing with geometric and physical implications of the constraints (4.15) and (4.16).

5. GEOMETRIC IMPLICATIONS OF THE ANALYTIC SOLUTIONS

For examining geometric properties of solutions of the Grad-Shafranov equation (4.12) subject to the constraints (4.15) and (4.16), let the set of particular solutions (4.18) be represented in the fixed cylindrical frame (R,Z,ϕ) by the constant-$\chi(\rho)$ surfaces

$$[R_m^2 - R^2]^2 + 4\, a^2 Z^2 R^2 = R_m^4\, \lambda(\rho) \ , \tag{5.1}$$

where

$$\lambda(\rho) \equiv \chi(\rho)/\psi_o \ . \tag{5.2}$$

Moreover, so that the formulae derived from (5.1) give analytically determined values readily comparable with numerically determined values, let all expressions be parameterized with respect to the main flux coordinate ρ. In

addition to being a flux-surface label, ρ is, as used here (or else is redefined to be), the half-width on the horizontal midplane of the vertical cross section of the flux surface $\chi(\rho)$; i.e., ρ is a measure of minor radius and has the units of length (see Figs. 1 and 2).

The first property to be deduced from (5.1) is that the maximum real value of R for the surface corresponding to a given $\lambda(\rho)$ must be

$$\max R^2(\rho) \equiv R_2^2(\rho) = R_m^2 \left[1 + \lambda(\rho)^{1/2}\right], \tag{5.3a}$$

which corresponds to a point where $Z^2 = 0$. It is, of course, customary to define major and minor radii as lying on the horizontal midplane where $Z^2 = 0$. Accordingly, for the surface corresponding to $\lambda(\rho)$ the minimum value of R for $Z^2 = 0$ is found to be

$$\min R^2(\rho) \equiv R_1^2(\rho) = R_m^2 \left[1 - \lambda(\rho)^{1/2}\right]. \tag{5.3b}$$

Because of the way ρ is defined (i.e., the half-width of the flux surface on the horizontal midplane)

$$\rho = \tfrac{1}{2}\left[R_2(\rho) - R_1(\rho)\right], \tag{5.4}$$

while the major radius $R_G(\rho)$ of the flux surface labeled ρ is naturally defined to be

$$R_G(\rho) = \tfrac{1}{2}\left[R_2(\rho) + R_1(\rho)\right]. \tag{5.5}$$

It immediately follows that

$$R_G^2(\rho) + \rho^2 = R_m^2 , \qquad \text{for } \rho \in [0,a] \tag{5.6}$$

and from (5.3a) and (5.3b)

$$\lambda(\rho) = \left(\frac{2\,\rho\,R_G(\rho)}{R_m^2}\right)^2 = \frac{4\,\rho^2}{R_m^4}\left(R_m^2 - \rho^2\right) , \tag{5.7}$$

where, since in general $R_G^2(\rho) + \rho^2 - 2\,\rho\,R_G(\rho) \geq 0$,

$$0 < \lambda(\rho) \leq 1 \quad \text{for } \rho \in (0,a]. \tag{5.8}$$

Moreover, for $\rho \in (0,a]$

$$\frac{d\lambda(\rho)}{d\rho} > 0 \quad \text{if } R_m > \sqrt{2}\,a , \tag{5.9}$$

so that for $\rho \in [|\Delta\rho|,a]$

$$0 \leq \lambda(\rho - |\Delta\rho|) \leq \lambda(\rho) \leq \lambda(a) \tag{5.10}$$

which corresponds to (4.22) and can be used in proving that a set of $\chi(\rho)$ surfaces defined by (5.1) is nested for surfaces having the same values of R_m and α^2.

To prove the nested property, note that, in view of (5.3a) and (5.3b), (5.1) can be rewritten as

$$Z^2 = \frac{\left[R_2^2(\rho) - R^2\right]\left[R^2 - R_I^2(\rho)\right]}{4\,\alpha^2 R^2} , \tag{5.11}$$

where from Eqs. (5.3a), (5.3b), and (5.10) it can be seen that $R_2^2(\rho)$ is a monotonic increasing function of ρ, and $R_1^2(\rho)$ a monotonic decreasing function of ρ. Consequently, due to the structure of (5.11), the surface corresponding to $\rho - |\Delta\rho|$ must be completely contained within the surface ρ, and this holds for any ρ in the range $[|\Delta\rho|,a]$. Thus, the set of $\chi(\rho)$-surfaces for given values of R_m and a^2 are nested with respect to ρ. Moreover, when the toroidal (or ϕ) direction is included, these nested surfaces become nested toroids and, since from Eqs. (5.3a), (5.3b), and (5.7)

$$\lim_{\rho\to 0} R_2^2(\rho) = \lim_{\rho\to 0} R_1^2(\rho) = R_m^2 \ , \tag{5.12}$$

as ρ approaches zero these toroids converge onto a closed loop (magnetic axis) of major radius R_m.

An interesting geometric property associated with these considerations is the shift $S(\rho)$ of the horizontal center of an arbitrary flux surface ρ relative to the magnetic axis (sometimes called the Shafranov shift):

$$S(\rho) = R_m - R_G(\rho) = R_m - \left(R_m^2 - \rho^2\right)^{1/2} \ . \tag{5.13}$$

As a measure of departure from circular cross sections, consider the maximum value of Z^2. This can be obtained from (5.1) by finding the value of Z^2 which makes $d(Z^2)/d(R^2)$ vanish and the corresponding second derivative negative. The result is

$$\max Z^2 \equiv \hat{Z}^2 = \left[R_m^2/\left(2\,a^2\right)\right]\left[1 - \left(1 - \lambda(\rho)\right)^{1/2}\right], \tag{5.14}$$

at the radial location

$$\hat{R}(\rho)^2 = R_m^2[1 - \lambda(\rho)]^{1/2} . \tag{5.15}$$

It is important to note that, if the geometric elongation is defined as $E(\rho) = |\hat{Z}(\rho)|/\rho$, then it follows from (5.14), (5.15), and (5.7) that

$$E^2(\rho) = [R_m^2/(2\,a^2\rho^2)][1 - (1 - \lambda(\rho))^{1/2}]$$

$$= 1/a^2 \qquad \text{for } \rho \in (0,a] , \tag{5.16}$$

which exhibits the nonphysical restriction that <u>the elongation must be the same for all nested analytic surfaces stemming from (5.1) and having the same value for a^2</u>.

A second measure of the departure from circularity is the geometric triangularity:

$$D(\rho) \equiv [R_G(\rho) - \hat{R}(\rho)]/\rho, \tag{5.17}$$

where $\hat{R}(\rho)$ [see (5.15)] is the radial location of the maximum Z^2. Starting from (5.17), the following alternative expressions for $D(\rho)$ can be derived:

$$D(\rho) = \frac{1}{\rho}\left(\frac{1}{2}[R_2(\rho) + R_1(\rho)] - [R_2(\rho)\,R_1(\rho)]^{1/2}\right) \tag{5.18}$$

$$= \frac{1}{\rho}\left(R_G(\rho) - [R_G(\rho)^2 - \rho^2]^{1/2}\right) \tag{5.19}$$

$$= [R_m/(2\rho)][(1 + \lambda(\rho)^{1/2})^{1/2} + (1 - \lambda(\rho)^{1/2})^{1/2}$$

$$- 2[1 - \lambda(\rho)]^{1/4}] \ , \tag{5.20}$$

and for small ρ

$$D(\rho) = \frac{1}{2} \frac{\rho}{R_G(\rho)} + O\left(\frac{\rho^3}{R_G(\rho)^3}\right). \tag{5.21}$$

Note that in attempting to allow an arbitrary prescription of D(a) difficulties can occur. As an example, suppose that

$$D(a) \equiv 0 \ . \tag{5.22}$$

It would then follow from (5.17), (5.15), (5.7), and (5.6) that either

$$\frac{a^2}{R_o^2} \to 0 \ , \qquad R_o \equiv R_G(a) \ , \tag{5.23}$$

or

$$a^2 = 2R_o^2 \ , \tag{5.24}$$

which for a toroidally confined plasma is not physically reasonable.

The final geometric property to be considered here is the total volume $V(\rho)$ enclosed by the flux surface ρ: this can be calculated analytically. Remembering to include the ϕ direction and employing the cylindrical coordinates (R,Z,ϕ),

$$V(\rho) = 4\pi \int_{R=R_1(\rho)}^{R_2(\rho)} R \, dR \int_{Z=0}^{Z(R)} dZ \qquad \text{for } \rho \in (0,a], \tag{5.25}$$

where $Z(R)$ is given by the positive square root of (5.11). Thus, for an arbitrary ρ

$$V(\rho) = \frac{2\pi}{|\alpha|} \int_{R=R_1(\rho)}^{R_2(\rho)} \left(R_2^2(\rho) - R^2\right)^{1/2} \left[R^2 - R_1^2(\rho)\right]^{1/2} dR \ , \qquad (5.26)$$

which can be evaluated in terms of complete elliptic integrals [e.g., see Eq. (3.155-1), p. 248, Ref. 16]:

$$V(\rho) = \frac{2\pi}{3} \frac{R_2(\rho)}{|\alpha|} \left\{\left[R_2^2(\rho) + R_1^2(\rho)\right] E(\pi/2,q) - 2\, R_1^2(\rho)\, F(\pi/2,q)\right\} \ , \qquad (5.27)$$

where

$$q^2 \equiv \frac{R_2^2(\rho) - R_1^2(\rho)}{R_2^2(\rho)} \ , \qquad (5.28)$$

and where $F(\pi/2,q)$ denotes the complete elliptic integral of the first kind and $E(\pi/2,q)$ the complete elliptic integral of the second kind.

In concluding this section on geometric properties note that, by prescribing merely (1) the major radius of the outer surface, $R_o \equiv R_G(a)$; (2) the minor radius (i.e., max $\rho = a$) along the horizontal midplane; and, (3) the geometric elongation $E(a)$ of the outer surface; it follows that the geometry of the family of nested analytic flux surfaces is completely determined. A review of the geometric quantities considered is set out below:

major radius of the outermost surface (prescribed)	$R_o = R_G(a)$
minor radius of the outermost surface (prescribed)	max $\rho = a$
major radius to the magnetic axis	$R_m = (R_o^2 + a^2)^{1/2}$
major radius of an arbitrary surface ρ	$R_G(\rho) = (R_m^2 - \rho^2)^{1/2}$
minor radius of an arbitrary surface ρ	ρ
(ρ is the principal parameter)	

maximum major radius of surface ρ	$R_2(\rho) = R_G(\rho) + \rho$
minimum major radius of surface ρ	$R_1(\rho) = R_G(\rho) - \rho$
lambda parameter of the arbitrary surface ρ	$\lambda(\rho) = \left(2\rho\ R_G(\rho)/R_m^2\right)^2$
Shafranov shift for the arbitrary surface ρ	$S(\rho) = R_m - R_G(\rho)$
geometric elongation of outermost surface [E(a) is prescribed]	$E(a)$
reciprocal elongation parameter α^2	$\alpha^2 = 1/E^2(a)$
geometric elongation of an arbitrary surface ρ	$E(\rho) = 1/\sqrt{\alpha^2}$
triangularity of an arbitrary surface ρ [D(p) is a dependent quantity]	$D(\rho) = 1/\rho\left(R_G(\rho) - \left[R_G^2(\rho) - \rho^2\right]^{1/2}\right)$
volume enclosed by an arbitrary surface ρ	$V(\rho) =$ Eq. (5.27)

6. PHYSICAL IMPLICATIONS OF THE ANALYTIC SOLUTIONS

Once again, the constraints on the Grad-Shafranov equation (4.12) that yield the simplest analytic solution are

$$A(\chi) = 2\pi c\ \frac{\partial P(\chi,t)}{\partial \chi} = \frac{2\pi c}{\chi'(\rho,t)}\ \frac{\partial P(\rho,t)}{\partial \rho} \equiv -A_o\ , \tag{6.1}$$

and

$$B(\chi) = \frac{c}{2}\ g(\chi,t)\ \frac{\partial g(\chi,t)}{\partial \chi} = \frac{c}{2}\ \frac{g(\rho,t)}{\chi'(\rho,t)}\ \frac{\partial g(\rho,t)}{\partial \rho} \equiv 0, \tag{6.2}$$

where $g(\rho,t)$ is the toroidal flux function

$$g(\rho,t) = R^2\left(\vec{B}\cdot\vec{\nabla}\phi\right), \tag{6.3}$$

and where sometimes "t" is omitted from the argument for convenience. Moreover, the relationship between the constant A_o and the lambda parameter of the analytic flux surface [see (4.19) and (5.2)] is given by

$$\lambda(\rho) \equiv \frac{\chi(\rho)}{\psi_o} = \frac{c}{\pi^2} \frac{1 + \alpha^2}{R_m^4} \frac{\chi(\rho)}{A_o} . \tag{6.4}$$

In this section consideration is given mainly to the physical significance of (6.1). As for (6.2), it implies that

$$\frac{\partial g(\rho,t)}{\partial \rho} \to 0 \tag{6.5}$$

or through (4.7)

$$\vec{J} \cdot \vec{\nabla} \theta \to 0. \tag{6.6}$$

The last condition [i.e., (6.5) and (6.6)] seems to make approximate sense in tokamak plasmas with highly symmetric vertical cross sections, but is not universal enough to allow neglecting $B(\chi)$ in the Grad-Shafranov equation. In instances where the vertical cross section is a nearly perfect ellipse [e.g., $D(a) \lesssim 0.01$, see Eq. (5.17)], it is found from the MHD part of a composite BALDUR-MHD code that

$$\frac{|B(\chi)|}{|A(\chi)R^2|} \lesssim 10^{-4}. \tag{6.7}$$

Otherwise, the above ratio may be $\lesssim 1/50$; hence, use of (6.2) introduces a degree of uncertainty when trying to match the analytic solutions against numerically determined solutions.

If (6.1) and (6.2) were both true, the Grad-Shafranov equation would reduce to [see (4.17)]

$$\Delta^{*}\chi = \frac{8\pi^2}{c} A_o R^2 \ , \tag{6.8}$$

and it would follow from (4.11) which defines Δ^{*}, and (4.8) which is an expression for $\vec{J}\cdot\vec{\nabla}\phi$, that

$$A_o = \vec{J}\cdot\vec{\nabla}\phi \ , \tag{6.9}$$

where $|\vec{J}\cdot\vec{\nabla}\phi| = J_\phi/R$ is a measure of toroidal current density. Incidentally, the general relation is

$$-J_\phi = A(\chi)\, R + B(\chi)\, R^{-1}. \tag{6.10}$$

But, since the toroidal current $I(\rho)$ is fundamentally given by

$$I(\rho) = \int_{\rho=o}^{\rho} \int_{\theta=o}^{2\pi} (\vec{J}\cdot\vec{\nabla}\phi)\, \sqrt{g}\, d\theta\, d\rho \ , \tag{6.11}$$

Eq. (6.9) implies that [see (5.25) for $V(\rho)$ and transform to (ρ,θ,ϕ)]

$$A_o = 2\pi \frac{I(\rho)}{V(\rho)} = 2\pi \frac{I_o}{V_o} \quad \text{for } \rho \in (0,a] \ , \tag{6.12}$$

where I_o denotes the total toroidal current (statamperes) flowing in a plasma of total volume $V_o(cm^3)$. When (6.12) is substituted into (4.19), the result is

$$\psi_o = \frac{2\pi^3}{c} \frac{R_m^4}{1 + \alpha^2} \frac{I_o}{V_o} \ . \tag{6.13}$$

However, in attempting to match a set of analytic solutions, the directness of the above equation does not imply that I_o can be prescribed arbitrarily. To be consistent, I_o must satisfy a relation obtained by integrating (6.1) with respect to χ subject to the condition that

$$\lim_{\rho \to o} \chi(\rho) = 0. \tag{6.14}$$

Thus, with the help of (6.12), it is found that

$$\frac{I_o}{V_o} = \frac{c}{\chi(\rho)} \left[P_o - P(\rho)\right] \quad \text{for } \rho \in (0,a], \tag{6.15}$$

where P_o [see Eq. (3.5)] denotes the plasma pressure (ergs/cm^3) at the magnetic axis and $P(\rho)$ the pressure on an arbitrary flux surface ρ. Evidently, $[P_o - P(\rho)]/\chi(\rho)$ must be constant with respect to ρ in order to satisfy the constraint (6.1); consequently, I_o and P_o cannot be prescribed independently.

According to the analytically determined expression for $\lambda(\rho) \equiv \chi(\rho)/\psi_o$ [i.e., Eq. (5.7)], it can be shown that, due to the constancy of $[P_o - P(\rho)]/\chi(\rho)$, the pressure profile corresponding to these simple analytic solutions is given by

$$P(\rho) = P_o - \frac{P_o - P(a)}{a^2 R_o^2} \rho^2 \left(R_m^2 - \rho^2\right), \tag{6.16}$$

where $P(\rho)$ is in units of ergs/cm^3, and the negative pressure gradient is given by

$$-\frac{\partial P(\rho)}{\partial \rho} = \frac{P_o - P(a)}{a^2 R_o^2} 2\rho \left(R_m^2 - 2\rho^2\right), \tag{6.17}$$

both expressions, of course, stem from (6.1). Note that the negative pressure gradient, $-\partial P/\partial\rho$, exhibits its maximum value of

$$\max_{\rho}\left[-\frac{\partial P(\rho)}{\partial\rho}\right] = \left(\frac{2}{3}\right)^{3/2}\frac{P_o - P(a)}{a^2 R_o^2}R_m^3 , \tag{6.18}$$

at

$$\rho = \rho_m = \frac{1}{\sqrt{6}}R_m , \tag{6.19}$$

provided $R_m/\sqrt{6} \le a$.

The restraint on toroidal current I_o is made more obvious by combining (6.13) and (6.15) with $\chi(\rho) = \lambda(\rho)\,\psi_o$ and using the constancy of $[P_o - P(\rho)]/\chi(\rho)$ to yield

$$\left(\frac{I_o}{V_o}\right)^2 = \frac{c^2}{8\pi^3}\frac{1+\alpha^2}{a^2 R_o^2}\left[P_o - P(a)\right], \tag{6.20}$$

which shows that I_o is definitely determined once the central pressure P_o and surface pressure $P(a)$ are given along with three geometric properties of the outer surface: R_o, a, and $\alpha^2 = 1/E(a)^2$.

Another important property of the constraint (6.1) is that it leads to a simple <u>analytic</u> formula for $\chi'(\rho)$ which can be readily used to check noncircular <u>numerical</u> calculations of the poloidal flux density as they are carried out in the transport part of the BALDUR-MHD code. In particular, from (6.1)

$$\chi'(\rho,t) = \frac{2\pi c}{A_o}\left(-\frac{\partial P(\rho,t)}{\partial\rho}\right) . \tag{6.21}$$

This implies when (6.12) is substituted for A_o and (6.17) for the pressure gradient, that

$$\chi'(\rho,t) = \frac{c}{(I_o/V_o)} \frac{P_o - P(a)}{a^2 R_o^2} 2\rho \left(R_m^2 - 2\rho^2\right). \tag{6.22}$$

where $\chi'(\rho,t)$ is in units of gauss-cm. Incidentally, (6.22) shows that, in the neighborhood of $\rho = 0$, $\chi'(\rho,t)$ is directly proportional to ρ which agrees with physical inference.

Moreover, a second formula for $\chi'(\rho,t)$ can be derived starting from (6.1), but this involves a numerically determined geometric factor. To derive this second formula consider Eq. (6.8), which results from the substitution of (6.1) and (6.2) into the Grad-Shafranov equation. Then make use of a standard generalized formula for the divergence in order to express $\Delta^*\chi$ in terms of flux coordinates (ρ,θ,ϕ):

$$A_o = \frac{c}{8\pi^2}\left[\frac{1}{\sqrt{g}} \frac{\partial}{\partial\rho}\left(\frac{(\vec{\nabla}\rho)^2}{R^2} \chi'(\rho)\sqrt{g}\right) + \frac{1}{\sqrt{g}} \frac{\partial}{\partial\theta}\left(\frac{(\vec{\nabla}\rho\cdot\vec{\nabla}\theta)}{R^2} \chi'(\rho)\sqrt{g}\right)\right]. \tag{6.23}$$

Let this expression be multiplied by $\sqrt{g}$ and integrated over $\theta \in [0,2\pi]$. The procedure yields [see (3.20)]

$$A_o 2\pi \int_o^{2\pi} \sqrt{g}\, d\theta = A_o V'(\rho,t) = \frac{c}{4\pi} \frac{\partial}{\partial\rho}\left(\chi'(\rho) \int_o^{2\pi} \frac{(\vec{\nabla}\rho)^2}{R^2} \sqrt{g}\, d\theta\right). \tag{6.24}$$

Next, the above is integrated over ρ, noting that by (3.20) and (3.24) and by (4.2)

$$\lim_{\rho\to o} V'(\rho,t) = 0 \qquad \text{and} \qquad \lim_{\rho\to o} \chi'(\rho,t) = 0. \tag{6.25}$$

Using (3.21) and (6.12), the result obtained is

$$\chi'(\rho,t) = \frac{4\pi}{c}\frac{I_o}{V_o} V(\rho,t)/G_\theta(\rho,t), \tag{6.26}$$

where

$$G_\theta(\rho,t) \equiv \frac{1}{2\pi}\int_o^{2\pi} \frac{(\vec{\nabla}\rho)^2}{R^2}\sqrt{g}\, d\theta. \tag{6.27}$$

Alternative expressions for (6.26) are [see (7.35c)]

$$\chi'(\rho,t) = \frac{4\pi}{c} I(\rho,t)/G_\theta(\rho,t), \tag{6.28}$$

where $I(\rho,t)$ denotes the total toroidal current contained within the flux surface ρ, and

$$\tilde{\chi}'(\rho,t) \equiv \chi'(\rho,t)/(2\pi R_o) = \frac{2}{c}\frac{1}{R_o}\frac{I_o}{V_o}\frac{V(\rho,t)}{G_\theta(\rho,t)}, \tag{6.29}$$

where $(c/2)\ \tilde{\chi}'(\rho,t)$, expressed in "internal" code units, is the quantity calculated numerically in the BALDUR code. The significance of $\tilde{\chi}'(\rho,t)$ is that in the case of circular cross sections it reverts back to the poloidal magnetic field.

Note that these last formulae [(6.26) through (6.29)] are not pure extensions of the basic constraint (6.1) because they contain the geometric factor $G_\theta(\rho,t)$ which at present is evaluated numerically in the course of running the MHD subprogram. Also, there is another quantity involved: the volume $V(\rho,t)$ can either be handled analytically by means of Eq. (5.27) or evaluated numerically in the MHD subprogram; the last procedure is employed here. In fact, comparisons of results from (6.26) against (6.22) offer

further checks on the performance accuracy of the MHD subprogram.

In summary, use of the constraints (6.1) and (6.2) lead to tractable analytic solutions of the Grad-Shafranov equation (4.12), and yield a set of formulae that can be employed to check numerical methods for simulating toroidal plasmas of noncircular cross sections. However, for plasmas with highly distorted cross sections (e.g., triangularity > 0.3), difficulties arise in attempting to match real physical behavior to the conditions [i.e., (6.5) and (6.6)] implied by the constraint (6.2). There are apparently no other essential difficulties, only limitations on the choice of initial and boundary conditions needed to make the numerical model consistent with the analytic solutions. By way of an example, although the plasma pressure both on the magnetic axis and on the outer boundary can be prescribed largely arbitrarily, the pressure profile in between must exhibit a radial dependence which preserves the constancy of $[P_o - P(\rho)]/\chi(\rho)$; i.e., Eq. (6.16) is needed for analytic consistency. Finally, two formulae for the poloidal magnetic flux density $\chi(\rho,t)$ are presented: (1) one of these (6.22) is strictly analytic; and (2) the other (6.26) is part analytic and part numerical. It is "numerical" in the sense of involving the geometric quantity $G_\theta(\rho,t)$ determined in the MHD part of the BALDUR-MHD code. Perhaps the most important use of these two equations is to check the accuracy of the numerical method used to advance the poloidal flux density in the course of any normal BALDUR-MHD run. The governing equation for this third method is discussed in the next section, where it is shown that an explicit modification of the parallel resistivity [see (7.41)] can make this governing equation consistent with the analytic solutions which stem from (6.1) and (6.2).

7. EQUATION FOR ADVANCING POLOIDAL FLUX DENSITY AND A MODIFICATION MAKING IT CONSISTENT WITH THE ANALYTIC SOLUTIONS

The governing equation for advancing the poloidal magnetic flux density $\tilde{\chi}'(\rho,t) = \chi'(\rho,t)/(2\pi R_o)$ is set out below using the flux coordinates (ρ,θ,ϕ) [see (3.7) through (3.23)]:

$$\frac{\partial \tilde{\chi}'(\rho,t)}{\partial t} - \langle \vec{u}_g \cdot \vec{\nabla}\rho \rangle_f \frac{\partial \tilde{\chi}'(\rho,t)}{\partial \rho} = \frac{c^2}{4\pi} \frac{\partial}{\partial \rho} \left[\frac{\eta_\parallel}{V'} \frac{\partial}{\partial \rho} \left(V' \langle (\vec{\nabla}\rho)^2 \rangle_f \tilde{\chi}'(\rho,t) \right) \right]$$

$$- c \frac{\partial}{\partial \rho} \left[\left\langle \frac{R}{R_o} \right\rangle_f \eta_\parallel J_\phi(\text{non-ohmic}) \right]. \tag{7.1}$$

This equation applies on the region $\rho \in (0,a)$, and is solved subject to the boundary conditions

$$\tilde{\chi}'(0,t) = \chi'(0,t)/(2\pi R_o) = 0, \qquad \text{at} \quad \rho=0 \ , \tag{7.2}$$

and

$$\tilde{\chi}'(a,t) = \chi'(a,t)/(2\pi R_o) = \frac{2}{c} \frac{1}{R_o} \frac{I(a,t)}{G_\theta(a,t)} \ , \qquad \text{at} \quad \rho=a \ , \tag{7.3}$$

where $I(a,t)$ denotes the total toroidal current flowing in the plasma at a time t, R_o is the major radius out to the center of the outermost flux surface as projected on the horizontal midplane, $\vec{u}_g$ represents the local velocity of a point (ρ,θ,ϕ) relative to an inertial frame $\vec{x} = (R,Z,\phi)$, and

$$G_\theta(\rho,t) \equiv \frac{1}{2\pi} \int_o^{2\pi} \frac{(\vec{\nabla}\rho)^2}{R^2} \sqrt{g} \, d\theta \qquad \text{for } \rho \in [0,a]. \tag{7.4}$$

A normalized flux density $\tilde{\chi}'(\rho,t) \equiv \chi'(\rho,t)/(2\pi R_o)$ has been introduced to make Eq. (7.1) resemble the equation implemented earlier for advancing the poloidal magnetic field B_p in the 1-D version of the BALDUR transport code. In fact,

$$\left(\begin{array}{c}\text{limit of } \tilde{\chi}'(\rho,t) \text{ as the plasma} \\ \text{cross section becomes circular}\end{array}\right) = B_p(\rho,t) \tag{7.5}$$

while in general

$$B_p(\rho,\theta,t) = \frac{|\vec{\nabla}\rho|}{2\pi R}\,\chi'(\rho,t) = |\vec{\nabla}\rho|\,\frac{R_o}{R}\,\tilde{\chi}'(\rho,t)\ . \tag{7.6}$$

Incidentally, if the major radius R_o varies with time t, a term containing d $\ell n(R_o)/dt$ should be added to the left-hand side of (7.1).

The derivation of Eq. (7.1) begins with Faraday's law

$$-\left.\frac{\partial \vec{B}}{\partial t}\right|_{\vec{x}} = c(\vec{\nabla} \times \vec{E}), \tag{7.7}$$

where the partial time derivative is taken at a fixed point in an inertial frame $\vec{x} \equiv (R,Z,\phi)$. Prior to substitution into (7.7), the contravariant formula for magnetic field $\vec{B}$ [see (4.1) through (4.3)] is rewritten:

$$\vec{B} = -\frac{1}{2\pi}\,\vec{\nabla} \times \left(\chi(\rho,t)\vec{\nabla}\phi\right] + g(\rho,t)\vec{\nabla}\phi. \tag{7.8}$$

When the result of substituting (7.8) into (7.7) is subject to vector multiplication by $\vec{\nabla}\phi$, it is found that

$$\vec{\nabla}\phi \times \left(\vec{\nabla} \times \vec{A}\right) = 0, \tag{7.9}$$

where

$$\vec{A} \equiv -\frac{1}{2\pi}\left.\frac{\partial \chi}{\partial t}\right|_{\vec{x}} \vec{\nabla}\phi + c\vec{E}\ . \tag{7.10}$$

Because of toroidal symmetry and the special geometry of the nonorthogonal flux coordinates [i.e., Eqs. (3.11) through (3.14)], Eq. (7.9) becomes

$$\vec{\nabla}\phi \times (\vec{\nabla} \times \vec{A}) = \frac{1}{R^2}\left[\frac{\partial R^2(\vec{A}\cdot\vec{\nabla}\phi)}{\partial\rho}\,\vec{\nabla}\rho + \frac{\partial R^2(\vec{A}\cdot\vec{\nabla}\phi)}{\partial\theta}\,\vec{\nabla}\theta\right]$$

$$= \frac{1}{R^2}\,\vec{\nabla}\left[R^2(\vec{A}\cdot\vec{\nabla}\phi)\right] = 0\ , \tag{7.11}$$

which implies that the quantity $R^2\,(\vec{A}\cdot\vec{\nabla}\phi)$ is globally uniform; i.e.,

$$R^2(\vec{A}\cdot\vec{\nabla}\phi) = C_1(t), \tag{7.12}$$

where $C_1(t)$ is a function of t only and $\vec{A}$ is given by (7.10). On differentiation with respect to the flux coordinate ρ, (7.12) is found to yield [see (3.14)]

$$-\frac{1}{2\pi}\frac{\partial\chi'}{\partial t}\bigg|_{\vec{x}} + c\,\frac{\partial}{\partial\rho}\left[R^2(\vec{E}\cdot\vec{\nabla}\phi)\right] = 0. \tag{7.13}$$

To evaluate $\vec{E}\cdot\vec{\nabla}\phi$ use is made of Ohm's law (Refs. 13, 15, 17, and elsewhere)

$$\vec{E} = \vec{\eta}\cdot(\vec{J} - \vec{J}(\text{non-ohmic})) - \frac{1}{c}\,(\vec{v}\times\vec{B}) - \frac{1}{|e|\,n_e}\,\vec{\nabla}P_e\ , \tag{7.14}$$

where $\vec{v}$ represents an effective flow velocity and $\vec{\nabla}P_e$ denotes the gradient of the electron pressure. Due to prevalence of the pressure-balance condition [i.e., (3.2)], the gradient of the total plasma pressure must be perpendicular to $\vec{B}$, and this supports the assumption that the same condition prevails for the electron pressure:

$$\vec{B}\cdot\vec{\nabla}P_e \equiv 0. \tag{7.15}$$

In view of (7.15) and the identity $\vec{B}\cdot(\vec{\nabla} \times \vec{B}) = 0$, Eq. (7.14) yields

$$\vec{E}\cdot\vec{B} = \vec{Z}\cdot\vec{B}\ , \tag{7.16}$$

where

$$\vec{Z} \equiv \bar{\eta}\cdot\{\vec{J} - \vec{J}(\text{non-ohmic})\}. \tag{7.17}$$

An expression for $\vec{E}\cdot\vec{\nabla}\phi$ [i.e., Eq. (7.22)] is now worked out from (7.16). First, introduction of the contravariant formula for $\vec{B}$ [i.e., (4.1)] into (7.16) gives

$$\begin{aligned}\vec{E}\cdot\vec{\nabla}\phi &= \vec{Z}\cdot\vec{\nabla}\phi - \frac{\chi'(\rho,t)}{2\pi\, g(\rho,t)}(\vec{E} - \vec{Z})\cdot(\vec{\nabla}\phi \times \vec{\nabla}\rho) \\ &= \vec{Z}\cdot\vec{\nabla}\phi + \frac{\chi'(\rho,t)}{2\pi\, g(\rho,t)}\left[\frac{1}{c}(\vec{v} \times \vec{B}) + \frac{\vec{\nabla}P_e}{|e|\, n_e}\right]\cdot[\vec{\nabla}\phi \times \vec{\nabla}\rho].\end{aligned} \tag{7.18}$$

Then it follows from (7.15) and $\vec{B}\cdot\vec{\nabla}\rho = 0$ [i.e., (3.9)] that

$$\left[\frac{1}{c}(\vec{v} \times \vec{B}) + \frac{\vec{\nabla}P_e}{|e|\, n_e}\right]\cdot[\vec{\nabla}\phi \times \vec{\nabla}\rho] = -\frac{1}{c}(\vec{v}\cdot\vec{\nabla}\rho)(\vec{B}\cdot\vec{\nabla}\phi)\ . \tag{7.19}$$

But, the toroidal flux function $g(\rho,t)$ is given by [see (4.3)]

$$g(\rho,t) = R^2(\vec{B}\cdot\vec{\nabla}\phi), \tag{7.20}$$

and the magnitude of the poloidal magnetic field by

$$B_p(\rho,\theta,t) = \frac{\chi(\rho,t)}{2\pi} |\vec{\nabla}\phi \times \vec{\nabla}\rho| = \frac{|\vec{\nabla}\rho|}{2\pi R} \chi(\rho,t). \tag{7.21}$$

In view of Eqs. (7.19) through (7.21) and of the assumption $|\vec{J}(\text{non-ohmic})| \approx J_\phi(\text{non-ohmic})$, (7.18) can be rewritten as follows

$$\vec{E}\cdot\vec{\nabla}\phi = \eta_\parallel(\vec{J}\cdot\vec{\nabla}\phi) - \eta_\parallel \frac{1}{R} J_\phi(\text{non-ohmic}) - \frac{1}{c}\frac{B_p}{R}\frac{(\vec{v}\cdot\vec{\nabla}\rho)}{|\vec{\nabla}\rho|}, \tag{7.22}$$

in which use of the symbol "$\eta_\parallel$" in association with ϕ-components implies that $|B_\phi| >> |B_p|$.

The term in (7.22) involving $v_\perp = (\vec{v}\cdot\vec{\nabla}\rho)/(|\vec{\nabla}\rho|$ is neglected because of the following relations which are characteristic (e.g., see Hinton and Hazeltine, Ref. 13) of the time scale being handled in transport calculations. It is necessary for the validity of the basic equations being used that

$$\delta \equiv \rho/\ell n << 1, \tag{7.23}$$

where for the moment ρ now represents a typical gyroradius and ℓn denotes the pressure scale length

$$\ell n \equiv |\vec{\nabla} \ell n\ P|^{-1}. \tag{7.24}$$

Moreover, as pointed out in Ref. 13, the following basic equations are only correct to order $O(\delta)$:

$$\vec{\nabla}P - \frac{1}{c}\left(\vec{J} \times \vec{B}\right) = O(\delta), \tag{7.25a}$$

$$\vec{B}\cdot\vec{\nabla}P = O(\delta)\ , \tag{7.25b}$$

$$n(\rho,\theta) = \langle n(\rho)\rangle_f\ [1 + O(\delta)], \tag{7.25c}$$

$$T(\rho,\theta) = \langle T(\rho)\rangle_f\ [1 + O(\delta)], \tag{7.25d}$$

$$u_\perp/u_\parallel = O(\delta),\ \text{etc.}, \tag{7.25e}$$

where $n(\rho,\theta)$ is a typical local particle density; ρ is the principal flux coordinate again; $T(\rho,\theta)$ denotes a temperature; and, $\langle\ldots.\rangle_f$ denotes a flux-surface average. Under the condition that $B_\phi >> B_p$, which is usually valid for tokamaks,

$$u_\parallel \approx u_\phi = R\left(\vec{u}\cdot\vec{\nabla}\phi\right). \tag{7.26}$$

Hence, by (7.25e)

$$\bar{n}\,u_\perp = O(\delta)\,\bar{n}\,u_\parallel = O(\delta)\,\frac{R}{|e|}\sum_a e_a n_a\left(\vec{u}_a\cdot\vec{\nabla}\phi\right) = O(\delta)\,\frac{R}{|e|}\left(\vec{J}\cdot\vec{\nabla}\phi\right), \tag{7.27}$$

which shows that the error caused by neglecting the term involving ($u_\perp = (\vec{v}\cdot\vec{\nabla}\rho)/|\vec{\nabla}\rho|$ is the same order as the errors in the basic equations [e.g., (7.25a) through (7.25d)]. Consequently, the expression introduced into (7.13) for $\vec{E}\cdot\vec{\nabla}\phi$ reduces to

$$\vec{E}\cdot\vec{\nabla}\phi = \eta_\parallel\left(\vec{J}\cdot\vec{\nabla}\phi\right) - \eta_\parallel\frac{1}{R}J_\phi(\text{non-ohmic}), \tag{7.28}$$

in which $\vec{J}\cdot\vec{\nabla}\phi$ is related to $\chi'(\rho,t)$ according to (4.8).

Substitution of (4.8) for $\vec{J}\cdot\vec{\nabla}\phi$ into (7.28) and, in turn, substitution of the result into (7.13) yields

$$\left.\frac{\partial\chi'}{\partial t}\right|_{\vec{x}} = \frac{c^2}{4\pi}\frac{\partial}{\partial\rho}\left[R^2\eta_{\parallel}\,\vec{\nabla}\cdot\left(\frac{1}{R^2}\,\chi'(\rho,t)\,\vec{\nabla}\rho\right)\right] - 2\pi c\,\frac{\partial}{\partial\rho}\left[R\,\eta_{\parallel}\,J_{\phi}(\text{non-ohmic})\right]. \tag{7.29}$$

Simplification is possible by noting that

$$R^2\vec{\nabla}\cdot\left(\frac{1}{R^2}\,\chi'\vec{\nabla}\rho\right) = \vec{\nabla}\cdot\left(\chi'\vec{\nabla}\rho\right) - \frac{2}{R}\,\chi'\,\left(\vec{\nabla}\rho\cdot\vec{\nabla}R\right), \tag{7.30}$$

while due to the geometry of the coordinate systems (ρ,θ,ϕ) and (R,Z,ϕ)

$$-\frac{2}{R}\,\vec{\nabla}\rho\cdot\vec{\nabla}R = 2\,\frac{\partial Z}{\partial\theta}/\sqrt{g}\ . \tag{7.31}$$

The flux-surface averaging of (7.29) is now carried out, remembering that by its nature $\chi'(\rho,t)$ is independent of θ; while, $\eta_{\parallel} = \eta_{\parallel}(\rho,t)$ and $J_{\phi}(\text{non-ohmic})$ are taken to already represent flux-surface-averaged properties. Use is also made of the following general theorem [see (3.18) through (3.23)]:

$$\langle\vec{\nabla}\cdot\vec{A}\rangle_f = \frac{1}{V'}\,\frac{\partial}{\partial\rho}\left(V'\langle\vec{A}\cdot\vec{\nabla}\rho\rangle_f\right). \tag{7.32}$$

Moreover, the partial time derivative of χ' is transformed <u>from</u> a point fixed in the (R,Z,ϕ) frame <u>to</u> the time derivative of χ' at a point fixed in the (ρ,θ,ϕ) frame, where $\vec{u}_g(\rho,\theta,\phi,t)$ denotes the velocity of the point (ρ,θ,ϕ) with respect to the (R,Z,ϕ) frame:

$$\left.\frac{\partial}{\partial t}\right|_{\vec{x}} = \left.\frac{\partial}{\partial t}\right|_{\rho,\theta} - \vec{u}_g(\rho,\theta,\phi,t)\cdot\vec{\nabla}. \tag{7.33}$$

The result of these relationships is that, when subjected to flux-surface averaging, Eq. (7.29) becomes

$$\frac{\partial \chi'(\rho,t)}{\partial t} - \langle \vec{u}_g\cdot\vec{\nabla}\rho\rangle_f \frac{\partial \chi'(\rho,t)}{\partial \rho} = \frac{c^2}{4\pi}\frac{\partial}{\partial \rho}\left[\frac{\eta_\parallel}{V'}\frac{\partial}{\partial \rho}\left(V'\langle(\vec{\nabla}\rho)^2\rangle_f \chi'(\rho,t)\right)\right]$$

$$- 2\pi c \frac{\partial}{\partial \rho}\left[\langle R\rangle_f \eta_\parallel J_\phi(\text{non-ohmic})\right], \tag{7.34}$$

which when normalized by dividing through by $2\pi R_o$ yields (7.1). Some slight modification in the left-hand side of (7.1) is, of course, needed if R_o is a function of time t.

Note that, once $\chi'(\rho,t)$ is known as a function of ρ, the toroidal current $I(\rho,t)$ at time t enclosed by the toroidal flux surface corresponding to ρ is implied. This can be seen by substituting Eq. (4.8) into the fundamental expression for toroidal current:

$$I(\rho,t) = \int_{\rho=0}^{\rho}\int_{\theta=0}^{2\pi}\left(\vec{J}\cdot\vec{\nabla}\phi\right)\sqrt{g}\,d\theta\,d\rho. \tag{7.34b}$$

Equation (4.8) is set out again here for convenience. In terms of the flux coordinates [see Eqs. (3.9) through (3.14)], Ampere's law [i.e., (3.3)] yields

$$\vec{J}\cdot\vec{\nabla}\phi = \frac{c}{8\pi^2}\vec{\nabla}\cdot\left[\frac{1}{R^2}\,2\pi\left(\vec{B}\cdot\vec{\nabla}\theta\right)\sqrt{g}\,\vec{\nabla}\rho\right], \tag{7.34c}$$

which for axisymmetric systems (where $\vec{\nabla}\cdot\vec{B} = 0$) can be written as in (4.8)

$$\vec{J}\cdot\vec{\nabla}\phi = \frac{c}{8\pi^2}\vec{\nabla}\cdot\left(\frac{1}{R^2}\,\chi'(\rho,t)\,\vec{\nabla}\rho\right). \tag{7.35}$$

Equation (7.35) can be substituted into (7.34b) and simplifications made using the general theorem given in (7.32) as well as the following relation due to (3.24); also see (6.25)

$$\lim_{\rho \to o} V'(\rho,t) = 0. \tag{7.35b}$$

The result is a formula for the toroidal current $I(\rho,t)$ in terms of the poloidal flux density $\chi'(\rho,t)$ and a geometric factor $G_\theta(\rho,t)$ defined in (7.4):

$$I(\rho,t) = \frac{c}{4\pi} \chi'(\rho,t)\, G_\theta(\rho,t). \tag{7.35c}$$

The necessary modification of Eq. (7.1), or of (7.34), in order to attain consistency with the analytic solutions is now examined. Under stationary conditions where $\partial\chi'/\partial t\big|_{\vec{x}} = 0$ and when $J_\phi(\text{non-ohmic}) = 0$, Eq. (7.34) reduces to

$$\frac{\partial}{\partial\rho}\left[\frac{\eta_\parallel}{V'}\frac{\partial}{\partial\rho}\left[V'\langle(\vec{\nabla}\rho)^2\rangle_f\, \chi'(\rho,t)\right]\right] = 0. \tag{7.36}$$

On the other hand, the analytic solutions demand that [see (6.8), (6.9), etc.]

$$\vec{J}\cdot\vec{\nabla}\phi = A_o\ , \tag{7.37}$$

which when combined with (7.35) gives (6.8); i.e.,

$$R^2\,\vec{\nabla}\cdot\left(\frac{1}{R^2}\,\chi'(\rho,t)\,\vec{\nabla}\rho\right) = \frac{8\pi^2}{c} A_o R^2. \tag{7.38}$$

Before being compared one-to-one with (7.36), the above expression must be subjected to flux-surface averaging; and, this involves making use again of Eqs. (7.30) through (7.32) with the result that (7.38) becomes

$$\frac{1}{V'}\frac{\partial}{\partial\rho}\left(V'\langle(\vec{\nabla}\rho)^2\rangle_f\,\chi'(\rho,t)\right) = \frac{8\pi^2}{c}A_o\langle R^2\rangle_f\ . \tag{7.39}$$

which immediately implies that, in the case of the analytic solutions

$$\frac{\partial}{\partial\rho}\left[\frac{1}{\langle R^2\rangle_f}\frac{1}{V'}\frac{\partial}{\partial\rho}\left(V'\langle(\vec{\nabla}\rho)^2\rangle_f\,\chi'(\rho,t)\right)\right] = 0. \tag{7.40}$$

On comparing (7.40) with (7.36), where the latter is derived from physical principles, it is seen that the governing equation for advancing poloidal magnetic flux density becomes consistent with the analytic solutions when the following condition is imposed on plasma resistivity:

$$\eta_{\parallel} \equiv \frac{\eta_o}{\langle R^2\rangle_f}\ , \tag{7.41}$$

where η_o is some convenient normalizing constant.

As a consequence of introducing the modification shown in (7.41), numerical results obtained using Eqs. (7.1) through (7.3), which are the equations programmed into the transport part of the BALDUR-MHD code, can be checked against Eq. (6.22), which is wholly analytic, and against Eq. (6.29), which is part analytic and part numerical.

8. ANALYTIC CHECKS OF A 1-1/2-D BALDUR TRANSPORT CODE

A. Description of the 1-1/2-D Transport Code

A composite 1-1/2-D transport code (the "BALDUR-VMOMS" code) for the numerical modeling of noncircular, magnetically confined toroidal plasmas has been assembled (Ref. 8) by linking a MHD-equilibrium program (Refs. 11 and 18) to a geometrically generalized version of the BALDUR transport code (Refs. 1 and 2). Toroidal symmetry and reasonably well nested flux surfaces are assumed to exist throughout the model. The transport part of this composite code is 1-D; it simulates cross-field transport in multispecies plasmas on a resistive time scale (Refs. 12-14, etc.), and executes numerical calculations of the time evolution of flux-surface-averaged quantities as a function of a principal flux-surface coordinate ρ (see Sec. 3). The MHD subprogram is 2-D and includes the determination at successive times of the Jacobian and other metrics of a flux-surface coordinate system (ρ,θ) based on the Grad-Shafranov equation (see Sec. 4). On the time scale being represented, most of the interesting plasma properties approach uniformity over any flux surface ρ so that it makes sense to eliminate the θ-dependence by flux-surface averaging [see (3.18)]. Although the transport equations in the BALDUR part of the code remain 1-D, they have been generalized so as to hold in nonorthogonal flux-coordinate space. The fundamental theorem used to carry out this generalization is set out in Eq. (3.23).

Any continuous changes in the flux-surface geometry are approximated, starting from time-zero, by stepwise changes implemented through successive calls to the MHD package. Interactions between the MHD and transport parts take place only while the MHD part is being called. Once the overall code is initialized in a self-consistent manner, MHD calls are only made every so many prescribed transport time steps or whenever plasma properties display

appreciable change. Between successive calls, changes in profiles of plasma density, pressure, poloidal-flux density, etc., due to transport are calculated with respect to flux-surface coordinates which are momentarily held fixed. This stepwise scheme removes from the transport equations convective-like terms associated with partial time derivatives. But, in this case of course, the transport coefficients should be measured with respect to the laboratory frame. The treatment is made physically valid by renormalizing the principal plasma properties after each flux-coordinate recalculation so as to conserve particles, entropy, and rotational transform with respect to toroidal-flux surfaces, where the rotational transform is given by $\iota = 2\pi \partial\chi/\partial\Phi$, χ being poloidal flux, Φ toroidal flux.

In the course of renormalization, the fundamental variations with respect to toroidal flux Φ are always preserved:

$$\text{(particles)} \quad n V' = f_1(\Phi), \tag{8.1}$$

$$\text{(entropy)} \quad p [V']^{5/3} = f_2(\Phi) , \tag{8.2}$$

$$\text{(rotational transform)} \quad \iota = f_3(\Phi) . \tag{8.3}$$

However, MHD subprogram calls generally induce changes both in the spacewise profile of toroidal flux Φ with respect to, say, the dimensionless horizontal minor radius $x \in [0,1]$ and in the volume gradient $V'(x,t)$ [see (3.20)]. Knowing the new spatial dependencies for Φ and V', as well as the invariant properties exhibited by (8.1) through (8.3), new self-consistent radial profiles for particle densities, plasma pressure, and poloidal-flux density,

$$\chi'(\rho,t) \equiv \frac{\partial \chi}{\partial \rho} = \frac{1}{2\pi} \iota \frac{\partial \Phi}{\partial \rho} , \tag{8.4}$$

can be determined immediately. These redetermined profiles are then used as new initial conditions from which to carry forward the transport calculations.

At time of writing, many of the original source and sink terms, although approximately representative for mildly noncircular cross sections, remain to be upgraded. However, the treatment of ohmic heating has been made more explicit than in earlier versions of the BALDUR code, the basic physical expression being

$$\langle \text{Ohmic heating rate} \rangle_f = \langle \vec{J} \cdot \vec{\eta} \cdot [\vec{J} - \vec{J}(\text{non-ohmic})] \rangle_f - \frac{1}{c} \langle \vec{J} \cdot (\vec{v} \times \vec{B}) \rangle_f , \tag{8.5}$$

where the electric field is given by (e.g., see Ref. 17)

$$\vec{E} = \vec{\eta} \cdot [\vec{J} - \vec{J}(\text{non-ohmic})] - \frac{1}{c} (\vec{v} \times \vec{B}) - \frac{\vec{\nabla} P_e}{e\, n_e} , \tag{8.6}$$

P_e denoting electron pressure [see (3.5)] and n_e electron density. In view of the pressure-balance condition [see (3.2) and (3.8)], it makes sense to write

$$-\frac{1}{c} \langle \vec{J} \cdot (\vec{v} \times \vec{B}) \rangle_f - \frac{1}{e\, n_e} \langle \vec{J} \cdot \vec{\nabla} P_e \rangle_f = +\frac{1}{c} \langle \vec{v} \cdot (\vec{J} \times \vec{B}) \rangle_f = \langle \vec{v} \cdot \vec{\nabla} \rho \rangle_f \frac{\partial P}{\partial \rho} . \tag{8.7}$$

Moreover, assuming ambipolarity the last term can be approximated by

$$\langle \vec{v} \cdot \vec{\nabla} \rho \rangle_f \frac{\partial P}{\partial \rho} = \frac{\Gamma_e}{n_e} \langle |\vec{\nabla} \rho| \rangle_f \frac{\partial P}{\partial \rho} , \tag{8.8}$$

where Γ_e denotes the surface-averaged cross-field electron particle flux in the direction of $\vec{\nabla}\rho$ and measured in the laboratory frame. Another aspect that has been fully upgraded, makes use of Eqs. (7.1), (7.2), and (7.3) to advance the poloidal magnetic-flux density, $\chi'(\rho,t)$ versus ρ, where $\chi'(\rho,t)$ of course determines $I(\rho,t)$, which is the toroidal current enclosed by the flux surface $\chi(\rho,t)$ [see Eq. (7.35c)]. Incidentally, this toroidal current profile together with the plasma pressure profile and the definition of the outermost boundary make up the time dependent input for the present MHD subprogram.

Consider the nature of the MHD subprogram (i.e., "VMOMS" of Ref. 18): It calculates the geometric relationships between the moving flux-surface coordinates (ρ,θ,ϕ) and the fixed cylindrical space (R,Z,ϕ); and, in the process it tracks surfaces of constant toroidal flux $\Phi(\rho,t)$ and determines poloidal current as a function of the principal flux-surface coordinate ρ. In order to maximize computational speed, the transformation equations are presently limited to three Fourier components which can be written

$$R(\rho,\theta) \equiv R_o(\rho) - \rho\cos(\theta) + R_2(\rho)\cos(2\theta) , \tag{8.9}$$

and

$$Z(\rho,\theta) \equiv E_o(\rho)\left[\rho\sin(\theta) + R_2(\rho)\sin(2\theta)\right] , \tag{8.10}$$

where $R(\rho,\theta)$ denotes the local major radius and $Z(\rho,r)$ the vertical displacement from the horizontal midplane. The validity of writing $E_o(\rho)R_n(\rho)$ for what otherwise might be $Z_n(\rho)$ [see (3.15) and (3.16)] is discussed by H. Weitzner in an appendix to Ref. 11. Typical configurations represented by (8.9) and (8.10) are shown in Figs. 1 and 2. Note that the principal coordinate ρ is taken to be the horizontal half-width of the particular flux surface corresponding to ρ [see Eq. (5.4)]:

$$\rho \equiv \frac{1}{2}\left[R(\rho,\pi) - R(\rho,0)\right] , \tag{8.11}$$

while the major radius of this surface is defined to be [see Eq. (5.5) and (8.9)]

$$R_G(\rho) \equiv \frac{1}{2}\left[R(\rho,\pi) + R(\rho,0)\right] = R_o(\rho) + R_2(\rho) , \tag{8.12}$$

and the magnetic axis R_m is located at

$$R_m = \lim_{\rho \to o} R_G(\rho) . \tag{8.13}$$

Although $E_o(\rho)$ and $R_2(\rho)$ are measures of elongation and triangularity, respectively, they are not quite the same as the $E(\rho)$ and $D(\rho)$ given in Eqs. (5.16) and (5.19) (see Ref. 18).

The present calculations of the Fourier coefficients [i.e., $R_o(\rho)$, $E_o(\rho)$, and $R_2(\rho)$] are based on a variational principle, in which the variation of the volume integral of a Lagrangian taken out to a prescribed boundary is assumed to vanish, thereby determining a best global fit and yielding an Euler equation which for the proper Lagrangian is equivalent to the Grad-Shafranov equation [e.g., (4.12)]. In practice, the variational principle is reformulated in terms of the Fourier components [e.g., $R_o(\rho)$, $E_o(\rho)$, and $R_2(\rho)$] so as to yield a separate Euler equation for each component. These equations are then averaged over the poloidal angle θ and treated as a set of coupled moment equations, which are solved simultaneously for the Fourier coefficients. In summary, the constraints imposed on the variational principle are: (1) definition of the outer boundary; (2) $I(\rho)$ versus ρ; and

(3) $P(\rho)$ versus ρ. Of course, there are other ways of setting up flux-surface coordinates based on the Grad-Shafranov equation, but the approach used here yields computationally fast algorithms.

Once the coefficients in Eqs. (8.9) and (8.10) are known, they are used to calculate the flux-surface averages [see Eq. (3.18)] of certain quantities needed to express the transport equations in terms of the flux-coordinate space [these factors include: $V'(\rho,t)$ as in (3.20), $\langle|\vec{\nabla}\rho|\rangle_f$, $\langle(\vec{\nabla}\rho)^2\rangle_f$, $G_\theta(\rho,t)$ as in (7.4), $\langle R/R_o\rangle_f$, $\langle R^2\rangle_f$, etc.]. Moreover, a modified form of the Grad-Shafranov equation [see Eq. (3.8) of Ref. 18] is used to calculate a special surface function, $f(\rho,t)$, which is a measure of poloidal current and which yields the toroidal flux function [see (4.3)] according to the formula

$$g(\rho,t) = R_o B_T(R_o)\, f(\rho,t) , \tag{8.14}$$

as well as

$$\frac{\partial g(\rho,t)}{\partial \rho} = R_o B_T(R_o) \frac{\partial f(\rho,t)}{\partial \rho} , \tag{8.15}$$

where $B_T(R_o)$ denotes the vacuum toroidal field at the point $R = R_o$, $Z=0$, and R_o is the major radius [see (8.12)] of the outermost flux surface. Equations (8.14) and (8.15) constitute the origin of the code-calculated values for the second Grad-Shafranov source term in Eq. (4.12):

$$B(\chi) \equiv \frac{c}{2} \frac{g(\rho,t)}{\chi(\rho,t)} \frac{\partial g(\rho,t)}{\partial \rho} . \tag{8.16}$$

Typical values for $B(\chi)$ as determined by the MHD subprogram are displayed in Tables 1 and 2. Note that, in view of Eqs. (3.24) and (4.7), in the

neighborhood of the magnetic axis

$$\lim_{\rho\to 0} \frac{\partial g(\rho,t)}{\partial \rho} = \lim_{\rho\to 0} \left\{ - \left[\frac{2}{c} \int_{\theta=0}^{2\pi} (\vec{J}\cdot\vec{\nabla}\theta)\, \sqrt{\bar{g}}\, d\theta \right] \right\} = 0 \ , \qquad (8.17)$$

and this property has been built into the code, where $g(\rho,t)$ is given by (4.3) and $\sqrt{\bar{g}}$ denotes the Jacobian.

The performance accuracy of the MHD part of this first BALDUR-MHD code, as well as the accuracy of the numerical calculations of $\chi(\rho,t)$ versus ρ, has been tested using the analytic formulae derived in Secs. 5-7. In these tests, the operations of the code were made as consistent as possible with the special Grad-Shafranov analytic solutions, the properties of which are summarized below.

B. Summary of the Properties of the Analytic Test Criteria

First of all, there are the two constraints [i.e., (6.1) and (6.2)] which yield the simplest possible nontrivial set of analytic solutions to the Grad-Shafranov equation (see Refs. 6 and 7). The remaining analytic properties are classified into "assigned" and "implied" categories.

Assigned properties of the analytic solutions: The special analytic solutions described in the preceding sections permit a limited range of arbitrary adjustment which can be utilized by prescribing reasonable values for the following quantities:

R_o — The major radius (cm) to the center of the outermost flux surface as projected onto the horizontal midplane.

a — The minor radius (cm) of the outermost flux surface projected onto the horizontal midplane.

$E(a)$ — The maximum vertical displacement of the outermost flux

surface with respect to the horizontal midplane divided by the minor radius "a" [see Eq. (5.16)]; i.e., $E(a) = \max [Z(a)^2]^{1/2}/a$.

P_o The plasma pressure (ergs/cm^3) on the magnetic axis [i.e., at $R = R_m = (R_o^2 + a^2)^{1/2}$ and $Z = 0$].

$P(a)$ The plasma pressure (ergs/cm^3) on the outermost flux surface, where $\rho = a$.

Bz The toroidal component of the vacuum magnetic field (kilogauss) at the center of the outermost flux surface ($R = R_o$, $Z = 0$).

Note that by (6.15) P_o and $P(a)$ define I_o/V_o, which in turn defines ψ_o and A_o.

Implied properties of the analytic solutions: After the "assigned" properties have been prescribed, additional analytic properties necessarily follow. The latter, largely defined by the formulae given in Secs. 5 and 6, include:

(1) Geometric properties stemming from the Fourier coefficients exhibited in (8.9) and (8.10), see Sec. 5. Note that the triangularity given by Eqs. (5.18) through (5.20) is an implied property.

(2) The shape of the plasma-pressure profile as represented by (6.16).

(3) The total toroidal current as determined by (6.20).

(4) Profiles of poloidal magnetic-flux density [e.g., Eq. (6.22)] and of toroidal current [e.g., Eq. (7.35c)].

(5) The analytic self-consistent plasma resistivity as defined

by Eq. (7.41).

C. Temporary Code Modifications which Yield Consistency with the Analytic Solutions

For purposes of implementing comparisons with the special analytic solutions, two types of temporary modifications were made in the BALDUR-VMOMS code First, so that the analytic results would be available for printouts, certain formulae from Secs. 5 and 6 were programmed into the interface subroutine (i.e., subroutine XVMOMS), which links the transport and MHD parts of the code. Second, in order to approach consistency with the analytic solutions, the following minor changes were introduced: (1) the prescribed boundary triangularity D(a) was overridden so as to satisfy (5.19); (2) the total toroidal current was reset according to $I_o = V_o(I_o/V_o)$, where $V_o = V(a)$ was calculated from (5.27) and (I_o/V_o) from (6.20); (3) the profile of plasma pressure (and, hence its gradient) between $\rho = 0$ and $\rho = a$ was made to match Eq. (6.16), where P_o and $P(a)$ remained arbitrarily adjustable; (4) lastly, the plasma parallel resistivity $\eta_\parallel(\rho)$, as used with Eq. (7.1), was redefined as follows [see (7.41)]:

$$\eta_\parallel \equiv \frac{\eta_o}{\langle R^2 \rangle_f} . \tag{8.18}$$

Note that, in view of (5.2) and (5.7), Eq. (6.16) for the analytic pressure profile can be rewritten as

$$P_o - P(\rho) = [P_o - P(a)] \frac{4\rho^2(R_m^2 - \rho^2)}{R_m^4} \frac{R_m^4}{4\, a^2 R_o^2}$$

$$= [P_o - P(a)] \frac{\text{analytic } \chi(\rho)}{\text{analytic } \chi(a)} . \tag{8.19}$$

Consequently, to the extent that the use of (8.19) with (7.1) results in

$$\text{BALDUR } \chi(\rho) = \text{analytic } \chi(\rho) \qquad \text{for } \rho \in [0,a], \tag{8.20}$$

it follows that the code calculations must according to (8.19) and (8.20) yield

$$-\frac{\partial P(\chi)}{\partial \chi} = \text{constant}, \tag{8.21}$$

which is consistent with the first analytic constraint (6.1) [also, sec (4.12) through (4.16)]. However, the second analytic constraint [i.e., (6.2)] apparently could not be built into the code calculations, but was found a posteriori to be satisfied to a greater or lesser degree depending upon geometric conditions. Examples of just how well this second constraint was satisfied are shown in Tables 1 and 2, which display the best and worse results. Satisfaction is approached when for code-calculated values $|A(\chi)|\, R_G^2 \gg |B(\chi)|$.

In a search for the best agreement between code calculations and the second analytic constraint, two different ways were tried for determining the $I(\rho)$ profile which is input to the MHD subprogram. In the first, the toroidal current profile [$I(\rho)$ versus ρ] was obtained directly from the normalized poloidal flux density $\tilde{\chi}'(\rho) \equiv \chi'(\rho)/(2\pi R_o)$, which was calculated by solving numerically Eq. (7.1) using Eq. (8.18) and subject to the conditions

$$\tilde{\chi}'(0) \equiv 0 \qquad \text{for } \rho = 0\ , \tag{8.22}$$

$$\tilde{\chi}'(a) \equiv \frac{2}{c}\frac{I_o}{R_o}\frac{1}{G_\theta(a)} \qquad \text{for } \rho = a\ , \tag{8.23}$$

as well as

$$\frac{\partial \tilde{\chi}'(\rho,t)}{\partial t} \equiv 0 \qquad \text{for } \rho \in (0,a) , \tag{8.24}$$

where

$$G_\theta(\rho) \equiv \frac{1}{2\pi} \int_0^{2\pi} \frac{(\vec{\nabla}\rho)^2}{R^2} \sqrt{g}\, d\theta \quad \text{for } \rho \in [0,a] . \tag{8.25}$$

Once $\tilde{\chi}'(\rho)$ was determined, $I(\rho)$ versus ρ followed from the relation [see Eq. (7.35c)]

$$I(\rho) = \frac{G_\theta(\rho)\, \tilde{\chi}'(\rho)}{G_\theta(a)\, \tilde{\chi}'(a)} I_o = \frac{c}{2} R_\wedge\, G_\theta'\rho)\, \tilde{\chi}'(\rho). \tag{8.26}$$

This first method had the advantage of including the numerical treatment of Eq. (7.1) in test comparisons of code calculations against the analytic solution.

The second way of determining the $I(\rho)$ profile was completely analytic; it made use of the formula [see (6.12)]

$$I(\rho) = \left(\frac{I_o}{V_o}\right) V(\rho) , \tag{8.27}$$

in which (I_o/V_o) was obtained from (6.20) and $V(\rho)$ from (5.27). As it turned out in practice, the first way [involving (7.1)] usually yielded somewhat better agreement between code calculations and the analytic solutions.

D. Description of the Properties Checked Against Analytic Values

The particular quantities examined in the comparisons of code-calculated against analytic values will now be described. To a large extent these are

set out in Exhibits A and B, which display results from two typical test runs, one showing good the other poor agreement. The quantities set out there have the following meanings:

r ≡ ρ — denotes the local horizontal minor radius (cm), where $0 < \rho \leq a$.

p — denotes the local plasma pressure (eV/cm^3).

ai — represents $I(\rho)$, the toroidal current (amps) contained within the flux surface labeled by $r = \rho$.

shift — is the local code-calculated Shafranov shift, $R_m - R_G(\rho)$ in cms [see (8.12) and (8.13)].

elong — is the local code-calculated elongation; i.e., expressed as an equation for an array element, this is given by

elong(i) $= \max [Z(\rho_i)^2/\rho_i^2]^{1/2}$ (8.28)

where in the code "$\rho \to 0$" is usually approximated by a small value: $\min \rho \equiv \rho_1 > 0$.

triang — is the local code-calculated triangularity which is given by

triang(i) $= [R_G(\rho_i) - \hat{R}(\rho_i)]/\rho_i$ (8.29)

where $R_G(\rho_i)$ is defined as in (8.12) and $\hat{R}_{(\rho_i)}$ denotes the distance from toroidal center to the point of maximum vertical displacement above the horizontal midplane of the flux surface labeled ρ_i.

zshift — is the local analytic Shafranov shift (cm) defined as equal to $R_m - (R_m^2 - \rho^2)^{1/2}$, where $R_m^2 \equiv R_o^2 + a^2$ in which R_o denotes the prescribed major radius to

the center of the outermost flux surface and "a" is the prescribed horizontal minor radius of this surface.

zelong — is $E(\rho_i)$, the local geometric elongation as calculated from the analytic formula (5.16).

ztrang — is $D(\rho_i)$, the local geometric triangularity obtained from the analytic formula (5.19) using $R_G(\rho)^2 = R_m^2 - \rho^2$ and $R_m^2 = R_o^2 + a^2$.

zlambda — is the local analytic poloidal-flux parameter defined by (5.2) and calculated according to (5.7).

zvolmi — is the code-calculated sum from zero out to ρ_i of the toroidal volume elements between the consecutive flux surfaces which correspond one-to-one with the spatial numerical grid ρ_i/a = XBOUNI(i+1) (the units are 10^{-12} cms).

zradjs — is the local major radius (cm) corresponding to the local minor radius ρ and defined by (8.12).

zbpoli — is the local analytically determined normalized poloidal magnetic flux density, $\tilde{\chi}'(\rho) \equiv \chi'(\rho)/(2\pi R_o)$ calculated according to Eq. (6.22) and expressed in terms of BALDUR internal units (1 gauss = 0.1 internal units).

ybpoli — is the local normalized poloidal flux density $\tilde{\chi}'(\rho)$ in internal units, calculated from Eq. (6.29), which is part analytic and part numerical.

bpoli — is the local normalized poloidal flux density

$\tilde{\chi}^{\prime}(\rho)$ in internal units, calculated wholly numerically in the code using Eqs. (7.1), (7.2), and (7.3) with (8.18) substituted for the resistivity.

beta-pol — is the local poloidal beta; i.e., beta-pol = $\beta_p \equiv P/(8\pi B_p^2)$, where P is the plasma pressure in ergs/cm^3 and B_p the poloidal magnetic field in gauss [see (7.21)].

Incidentally, as regards their positioning on the BALDUR spatial grid, all the above-mentioned quantities have been programmed to be evaluated at "zone-boundary" points (see Ref. 1 or 2); i.e., at points defined by the array elements XBOUNI(i+1) $\equiv \rho_i/a$, where "i = 1" corresponds to $\rho/a = 0$ and where on the outer boundary XBOUNI(imax+1) $\equiv 1$. In BALDUR imax+1 $\equiv$ MZONES.

Besides the comparisons between quantities defined above, other checks against the analytic solutions were made by means of the NMFE Computer Center debugging utility program "DDT." Included in "DDT" read-outs were the following: (1) Comparisons were made between the major radius R_m out to the magnetic axis as defined analytically by $R_m^2 = R_o^2 + a^2$ versus the value determined numerically in the MHD subprogram and stored into the array element PARAM(1) = R_m/a (see Ref. 18). (2) Differences were sought between the plasma volumes calculated analytically from Eq. (5.27) and the volumes (i.e., zvolmi) determined numerically by summing the finite-difference volume elements. (3) Values of the code-calculated ratio defined immediately below were investigated as a function of ρ, where this ratio [see Eqs. (4.12) through (4.16)] is a measure of the departure of code calculations from the second analytic constraint (4.16) or (6.2):

$$\varepsilon(\rho) \equiv \frac{B(\chi)}{A(\chi)\, R^2}, \qquad \chi = \chi(\rho). \tag{8.30}$$

Because of its bearing on the validity of the special analytic solutions as test criteria, the magnitudes of $\varepsilon(\rho)$ were examined in some detail as exemplified by Tables 1 and 2, where Table 1 stems from the same test run as Exhibit A and Table 2 corresponds to Exhibit B. Note that the values of $\varepsilon(\rho)$ were determined a posteriori.

E. Performance Results of the BALDUR-VMOMS Code

The agreement levels between code-calculated and analytically determined values for the properties defined above, as well as the magnitudes of $\varepsilon(\rho)$ [see (8.30)], were checked over a range of assigned properties. Of particular interest was the maximum distortion of a plasma cross section that could be handled by the present MHD subprogram, where the distortion was measured by the triangularity $D(\rho)$ [see (8.29)]. Since $D(a)$ (which is the triangularity of the boundary) is set up to be an implied property of the analytic solutions, it can be prescribed indirectly by assigning values to R_o and "a." For example, from Eq. (5.19)

$$a = \frac{2\, R_o D(a)}{1 + D(a)^2}. \tag{8.31}$$

Hence, if it is assumed that, say, $R_o = 140$ cm and $D(a) = 0.40$, then

$$a = 96.55 \text{ cm}.$$

On submitting test runs in which D(a) ≈ 0.4, it immediately became evident that the numerical model in the MHD subprogram failed to converge when

$$D(a) > \text{critical } D(a) \equiv 0.4. \tag{8.32}$$

A marginal run did execute in which the assigned parameters were: R_o = 140. cm; a = 76.6 cm; E(a) = 1.60; P_o = 1.520e+18 eV/cm^3; P(a) = 4.615e+15 eV/cm^3; B_Z = 5.0 T; as well as min ρ/a = 0.02 and error criteria = 10^{-4}. This yielded D(a) = 0.40 and, as shown in Exhibit B, gave poor agreement with analytically determined values.

It was next discovered that use of the analytic formula (8.27) for determining the toroidal current profile yielded some increase in the size of ε(ρ) [see (8.30)] and worsened the agreement between code-calculated and analytic values, except for the triangularity D(ρ) where, for some reason, agreement became very slightly better. Incidentally, the flag used in the code to select the method of determining I(ρ) was: (1) "npdump(1)=0" for the method involving (7.1), (8.18), and (7.35c); and (2) "npdump(1)=1" for the method using Eq. (8.27).

In the course of these studies a point was soon reached where it was decided both to restrict the investigative range to

$$0 < D(a) < 0.4, \tag{8.33}$$

and to determine I(ρ) versus ρ from $\tilde{\chi}'(\rho)$ as calculated according to Eqs. (7.1), (7.2), and (7.3) using (8.18) for the plasma resistivity. Except for the use of (8.18), this is normal operation for the BALDUR-VMOMS code and also allows the normal transport calculation of $\tilde{\chi}'(\rho)$ to be tested.

As illustrated by the numbers displayed in Exhibits A and B, test runs under certain conditions yielded good agreement between code-calculated and analytically determined quantities, while under other conditions (notably greater triangular distortion) poor agreement was obtained. The former case (Case A) was taken as indicating that some things were being handled properly (e.g., the $\tilde{\chi}'(\rho)$ calculations showed good agreement between zbpoli, ybpoli, and bpoli) whereas the latter case (Case B) led to some trial-and-error attempts to optimize agreement. The results of these parameter studies are summarized below.

First, it was found that reducing certain error-limit criteria increased the level of agreement up to a point; the trend is indicated by the following table:

xerror*	xparer*	Level of Agreement	Remarks
10^{-2}	10^{-3}	poor	the default values
10^{-3}	10^{-3}	better**	
10^{-4}	10^{-4}	marginally better than above	used for Case B (i.e., Exhibit B, Table 2)

*Prescribed internal convergence tolerances.
**Corresponds to Exhibit A.

The prescribed quantities "xerror" and "xparer" are used to set error-limit criteria that terminate iterations carried out in the subroutines D01AG*, which are located in the MHD subprogram and contain the algorithms that determine the Fourier coefficients of Eqs. (8.9) and (8.10) (see Ref. 18).

Second, the number of discrete θ-grid points representing the poloidal-angle range $\theta \in [0,2\pi]$ was increased from 11 to 21. This increase produced no

appreciable change in the disagreement between code-calculated and analytic values.

Third, in certain of the code calculations, effects of a singularity at x ≡ ρ/a → 0 are avoided by setting the minimum value of x slightly greater than zero [i.e., min x ≡ xp(1) > 0, whereas max x ≡ xp(max i) ≡ 1.]. In Case B [i.e., D(a) = 0.34], the difference between using xp(1) = 0.01 and xp(1) = 0.02 was found to be almost negligible, while the use of xp(1) = 0.001 resulted in convergence difficulties. For Case A [E(a) = 2.0, D(a) = 0.0085], use of xp(1) = 0.01 yielded slightly better agreement [e.g., between code-calculated values of D(ρ) and analytic D(ρ)] than did the very small value xp(1) = 10^{-4}, the larger value of xp(1) being slightly better in overall accuracy and much preferable from the standpoint of computational speed.

Fourth, regarding the spatial grid, in test runs where R_o = 248 cm, a = 85 cm, E(a) = 1.6, P_o = 1.520e+18 eV/cm^3, P(a) = 4.615e+15 eV/cm^3, B_Z = 52.0 kilogauss, D(a) = 0.1767, xp(1) = 0.01, and xerror = xparer = 0.001, it was found that using 20 radial zones in the MHD subprogram gave results very little different than with 40 radial zones. The finer zoning yielded, in comparisons against analytic values, slightly better agreement for the elongation E(ρ) [see (8.28)] and the total plasma volume, but slightly poorer agreement than 20 zones for values of the Shafranov shift S(ρ) = $R_m - R_G(\rho)$ [see (8.12) and (8.13)] and triangularity D(ρ) [see (8.29)]. Note that the results set out in Exhibits A and B were determined using 20 radial MHD zones and 11 θ-grid points.

Fifth, effects of enhancing plasma pressure P(ρ,t) (as well as the pressure gradient) and/or the applied toroidal field $B_Z = B_T(R_o)$ were examined. The thought was that, since the ratio ε(ρ), as defined in (8.30), can be written [see (4.12) through (4.14), and (4.3)]

$$\epsilon(\rho) = \frac{1}{4\pi}\,\frac{g(\rho,t)}{R^2}\,\frac{\partial g(\rho,t)/\partial\rho}{\partial P(\rho,t)/\partial\rho} = \frac{(\hat{\vec{B}}\cdot\hat{\vec{\nabla}}\phi)}{4\pi}\,\frac{\partial g(\rho,t)/\partial\rho}{\partial P(\rho,t)/\partial\rho}\ , \tag{8.34}$$

perhaps some decrease in the size of $\epsilon(\rho)$ would ensue if an increase in $|\partial P(\rho,t)/\partial\rho|$ were not offset by an increase in $|\partial g(\rho,t)/\partial\rho|$, where from (4.3)

$$g(\rho,t) \equiv R^2\{\hat{\vec{B}}\cdot\hat{\vec{\nabla}}\phi\}\ . \tag{8.35}$$

In the code, $g(\rho,t)$ is normally determined by the poloidal-current function $f(\rho,t)$ [see (8.14) and (8.15)], while in the test runs $-\partial P(\rho,t)/\partial\rho$ was specially redefined so as to fit the analytic formula (6.17). However, when the plasma pressure [particularly $\partial P(\rho,t)/\partial\rho$] was everywhere enhanced by the factor ×100, the following changes were found to occur:

(1) All geometric properties remained the same.

(2) The calculated values of $\tilde{\chi}'(\rho,t) \equiv \chi'(\rho,t)/(2\pi R_0)$ increased everywhere by ×10; this included zbpoli, ybpoli, and bpoli versus ρ, and implies that A_0 changes [see (6.12) and (6.21)].

(3) The toroidal-current profile $I(\rho)$ increased by ×10 over the region $0 < \rho \leq a$.

(4) The safety factor, $q \equiv \Phi'/\chi'$, Φ' denoting toroidal flux density, was down by very nearly a factor of ×10.

(5) The gradient of the poloidal-current function, $\partial f(\rho,t)/\partial\rho$ was found to increase in size by ×100.

(6) The value of $\epsilon(\rho)$ over the region $0 < \rho \leq a$ remained essentially unchanged.

As it turns out, the above behavior can be directly explained in terms of the most fundamental equation of the MHD model; i.e., the pressure-balance equation [see (3.2)]:

$$\vec{\nabla}P = \frac{1}{c}\left[\vec{J} \times \vec{B}\right] . \tag{8.36}$$

The effects of enhancing the pressure gradient become apparent when Eq. (8.36) is rewritten as a formula for $\partial P(\rho,t)/\partial\rho$. Starting with Eq. (4.1) for $\vec{B}$ and (4.9) for $\vec{J}$, and using (3.8), (3.10), (3.13) as well as certain standard vector identities, it follows from (8.36) that

$$\frac{\partial P(\rho,t)}{\partial\rho} = \frac{1}{c}\left[\sqrt{g}\,\left(\vec{J}\cdot\vec{\nabla}\theta\right)\left(\vec{B}\cdot\vec{\nabla}\phi\right) - \frac{1}{2\pi}\,\chi'(\rho,t)\left(\vec{J}\cdot\vec{\nabla}\phi\right)\right] , \tag{8.37}$$

where $\sqrt{g}$ denotes the transformation Jacobian [i.e., (3.10)] which is not the same as the toroidal-flux function in (8.35). Furthermore, it follows from Ampere's law [i.e., Eq. (3.3)] that

$$\vec{J}\cdot\vec{\nabla}\theta = -\frac{c}{4\pi}\,\frac{1}{\sqrt{g}}\,\frac{\partial g(\rho,t)}{\partial\rho} \tag{8.38}$$

as well as [see (4.7) and (4.8)]

$$\vec{J}\cdot\vec{\nabla}\phi = \frac{c}{8\pi^2}\,\vec{\nabla}\cdot\left[\frac{1}{R^2}\,\chi'(\rho,t)\,\vec{\nabla}\rho\right]. \tag{8.39a}$$

In the strictly analytic case, Eq. (6.20) for $(I_o/V_o)^2$ implies that, if $P_o - P(a)$ is scaled as $\times 100$, then I_o/V_o must scale as $\times 10$; and, hence, according to (6.22) $\chi'(\rho,t)$ must also scale as $\times 10$. By comparison, in the general algorithm for $\chi'(\rho,t)$ [see Eqs. (7.1) - (7.3)], value levels are determined by the outer

boundary condition (7.3), which in these tests had been programmed to always match the analytic total toroidal current:

$$I_o \equiv I(a,t) = \int_{\rho=o}^{a} d\rho \int_{\theta=o}^{2\pi} (\vec{J}\cdot\vec{\nabla}\phi)\,\sqrt{g}\,d\theta$$

$$= \frac{c}{4\pi}\,\chi'(a,t)\,\frac{1}{2\pi}\int_{\theta=o}^{2\pi}\frac{(\vec{\nabla}\rho)^2}{R^2}\,\sqrt{g}\,d\theta \quad , \tag{8.39b}$$

where I_o/V_o was always set according to (6.20). Since it makes sense to assume that for a fixed outer flux surface the quantity $G_\theta(a)$, see (8.25) or (3.26), is insensitive to pressure, it follows from (8.39b) that, when I_c scales by $\times 10$, $\chi'(\rho,t)$ versus ρ must scale by $\times 10$. All this is consistent with Eq. (8.37). Thus, if $\partial P(\rho,t)/\partial\rho$ is everywhere enhanced by $\times 100$, then

(1) $\chi'(\rho,t)$ must be enhanced by $\times 10$,

(2) $\vec{J}\cdot\vec{\nabla}\phi$, and hence toroidal current $I(\rho,t)$, must be enhanced by $\times 10$, and

(3) $(\vec{B}\cdot\vec{\nabla}\phi)\,\partial g(\rho,t)/\partial\rho$ must be enhanced by $\times 100$.

The last term forms the numerator in Eq. (8.34) for $\varepsilon(\rho)$ and offsets the enhancement of the denominator, thereby leaving $\varepsilon(\rho)$ unchanged. Moreover, in test cases in which the applied vacuum toroidal field $B_Z \equiv B_T(R_o)$ remains fixed while $\partial P/\partial\rho$ is enhanced by $\times 100$, it follows from (8.37) on substituting (8.38) for $\vec{J}\cdot\vec{\nabla}\theta$ and on using (8.15) to relate $\partial g(\rho,t)/\partial\rho$ and $\partial f(\rho,t)/\partial\rho$ that since the value $\vec{B}\cdot\vec{\nabla}\phi$ in the plasma is not very different than the vacuum value $B_T(R_o)/R_o$, the term

$$\frac{\partial f(\rho,t)}{\partial\rho} = \frac{1}{R_o B_T(R_o)}\,\frac{\partial g(\rho,t)}{\partial\rho}$$

must be enhanced by approximately ×100. Obviously, according to first principles, the code was doing precisely what it should.

Finally, it can be noted that an increase in the applied toroidal field from B_Z = 5.0 T to 10.4 T made no significant difference in code-calculated and analytically determined values other than, of course, in the safety factor $q = \partial\Phi(\rho,t)/\partial\chi(\rho,t)$, $\Phi(\rho,t)$ denoting the toroidal flux enclosed by the surface ρ.

In conclusion, as illustrated by the numbers set out in Exhibit A and Table 1, cases involving toroidal plasmas with vertically symmetric noncircular cross sections are handled with good accuracy; e.g., $\lesssim$ 0.5 percent for geometric properties and $\lesssim$ 0.002 percent (or $\lesssim$ 1/50,000) for the poloidal magnetic flux density $\chi(\rho,t)$. As regards the latter, it is particularly gratifying to find that the determination of $\chi(\rho,t)$, based on Eqs. (7.1), (7.2), and (7.3), and using (8.18), has been checked to better than one part in 50,000 against the exact formula (6.22) which stems only from the Grad-Shafranov equation (4.12) and the first analytic constraint (4.15). Cases with appreciable triangular distortion D(a) do not fare so well, as illustrated by Exhibit F and Table 2. In fact, when D(a) > 0.4, where D(a) denotes the triangularity of the outermost surface, the VMOMS MHD subprogram often fails to converge. It is likely that this deficiency can be corrected by adding more Fourier components to the formulation of the transformation equations (8.9) and (8.10).

F. Evidence in Support of More Fourier Components

The failure of various adjustments (described above in Subsection E) to reduce appreciably observed discrepancies between code-calculated and analytically determined values suggests the need for more Fourier components

in the basic transformation equations (8.9) and (8.10). As further evidence for this notion, an argument will now be made that these discrepancies cannot be accounted for by a departure of the code calculations from the second analytic constraint [i.e., (4.16) or (6.2)].

The particular case analyzed (Case B, corresponding to Exhibit B and Table 2) is characterized by moderately high triangular distortion [i.e., D(a) ≈ 0.34] and yields poor agreement with analytic values. These values stem from analytic solutions of the Grad-Shafranov equation and are exact only if this equation is made subject to the constraints [see (4.12) through (4.17)]:

$$A(\chi) = \frac{2\pi c}{\chi(\rho,t)} \frac{\partial P(\rho,t)}{\partial \rho} \equiv -A_o \ , \tag{8.40}$$

and

$$B(\chi) = \frac{c}{2} \frac{g(\rho,t)}{\chi(\rho,t)} \frac{\partial g(\rho,t)}{\partial \rho} \equiv 0. \tag{8.41}$$

When under test, the code was, of course, always modified so as to satisfy (8.40), but no special changes were introduced to make it comply with (8.41). However, the departure of the code from (8.41) was always examined a posteriori and recorded as the ratio $\varepsilon(o)$ defined in (8.34).

Since the analytic solutions are highly tractable, the errors due to neglecting $B(\chi)$ are represented by perturbing the analytic solutions. In particular, let $B(\chi)$ be matched by an effectively equivalent variation of the parametric constant A_o [see (4.12) and (8.40)]:

$$-\frac{8\pi^2}{c}\left[A(\chi)R^2 + B(\chi)\right] \equiv +\frac{8\pi^2}{c}\left(A_o + \delta A_o\right)R^2 \ ,$$

or

$$\delta A_o \equiv -\frac{1}{R^2} B(\chi) \ , \tag{8.42}$$

where $B(\chi)$ comes from code-calculated quantities by way of Eqs. (8.14) through (8.16). The question to be answered is whether neglect of $B(\chi)$ in formulating the analytic solutions can account for the discrepancies between these and the code calculations. Let the discrepancies be exemplified by comparing code-calculated and analytically determined values of the Shafranov shift [see (8.12) and (8.13) as well as (5.13)],

$$S(\rho) = R_m - R_G(\rho) = R_m - \left(R_m^2 - \rho^2\right)^{1/2} , \tag{8.43}$$

and let the differences be measured by the ratio

$$\left(\frac{\Delta S(\rho)}{S(\rho)}\right)_\chi \equiv \frac{\text{numerical "}S(\rho)\text{"} - \text{analytic "}S(\rho)\text{"}}{\text{analytic "}S(\rho)\text{"}} . \tag{8.44}$$

A variation in the parameter A_o accompanied by a variation in $S(\rho)$ can, of course, be induced by varying $R_o = R_G(a)$ while everything else is held constant. However, without being any more explicit let $R_\sim$, the magnetic axis, be made subject to variation; then

$$\frac{\delta S(\rho)}{S(\rho)} = - \frac{\delta R_m}{R_G(\rho)} . \tag{8.45}$$

On the other hand, from Eqs. (5.7) and (6.4), it follows that [on assuming the elongation given by (5.16) to be fixed]

$$\frac{2\, R_m\, \delta R_m}{R_o^2} = \delta\left(\frac{\chi(a)}{A_o}\right) \Big/ \left(\frac{\chi(a)}{A_o}\right) . \tag{8.46}$$

Moreover, Eqs. (6.12) and (6.15) imply that

$$\frac{\chi(a)}{A_o} = 2\pi c \frac{P_o - P(a)}{A_o^2} , \tag{8.47}$$

where it makes sense to hold the central and outer values of plasma pressure constant, i.e., $P_o - P(a)$ constant. Consequently,

$$\delta\left(\frac{\chi(a)}{A_o}\right)/\left(\frac{\chi(a)}{A_o}\right) = -2 \frac{\delta A_o}{A_o} , \tag{8.48}$$

and in view of (8.45), (8.46), and (8.48)

$$\frac{\delta S(\rho)}{S(\rho)} = \frac{R_o^2}{R_m R_G(\rho)} \frac{\delta A_o}{A_o} . \tag{8.49}$$

The argument is now advanced that neglecting $B(\chi)$ in the analytic solutions is not sufficient to account for the observed discrepancies between these and code calculations if for $0 < \rho \leq a$

$$\left|\left(\frac{\Delta S(\rho)}{S(\rho)}\right)_\chi\right| >> \frac{R_o^2}{R_m R_G(\rho)} \frac{|B(\chi)|}{A_o R^2} , \tag{8.50}$$

where $\left(\Delta S(\rho)/S(\rho)\right)_\chi$ represents the observed discrepancies [see (8.44)] and where $B(\chi)$ is determined from (8.16) using code-calculated values.

Note that R in (8.50) is a function of ρ and θ as shown in (8.9); and, this dependency can be approximated by introducing two special ratios:

$$\bar{\epsilon}(\rho) \equiv \frac{B(\chi)}{A(\chi)\, R_G(\rho)^2} , \tag{8.51}$$

and

$$\hat{\epsilon}(\rho) \equiv \frac{B(\chi)}{A(\chi)[R_G(\rho) - \rho]^2} , \tag{8.52}$$

where $A(\chi) \equiv -A_o$ and where the minimum value of $R(\rho,\theta)$ with respect to θ is given by

$$\min_{\theta} R(\rho,\theta) = R_G(\rho) - \rho \ . \tag{8.53}$$

Corresponding to $\bar{\varepsilon}(\rho)$ and $\hat{\varepsilon}(\rho)$, respectively, are the following variations, expressing relative differences in the analytically determined Shafranov shift when the analytic solutions are readjusted just enough to compensate for the nonzero code-determined values of $B(\chi)$:

$$\left(\frac{\delta S}{S}\right)_{\bar{\varepsilon}} = \frac{R_o^2}{R_m R_G(\rho)} \bar{\varepsilon}(\rho) \ , \tag{8.54}$$

and

$$\left(\frac{\delta S}{S}\right)_{\hat{\varepsilon}} = \frac{R_o^2}{R_m R_G(\rho)} \hat{\varepsilon}(\rho) \ . \tag{8.55}$$

The above quantities are estimates of the right-hand side of (8.50), and were evaluated (see Table 3) from the same test run that was used to yield Exhibit B and Table 2 [i.e., from Case B in which $D(a) \approx 0.34$]. The purpose of Table 3, of course, is to display a comparison between the left-hand and right-hand side of the critical relation (8.50). Column 2 of Table 3 sets up the horizontal minor radii ρ. Column 3 shows the observed relative discrepancies between code-calculated and analytically determined values of the Shafranov shift for Case B. Columns 5 and 6 contain the code-calculated mean and maximum ratios for the relative importance of $B(\chi)$ [see (4.12) and (8.51)]. Corresponding to the values in columns 5 and 6, columns 7 and 8 display the relative discrepancies in Shafranov shift estimated from the failure to include $B(\chi)$ in the analytic solutions. The extent in Table 3 to

which the inequality (8.50) is satisfied obviously implies that the omission of $B(\chi)$ in formulating the analytic solutions cannot fully account for the observed disagreement between code-calculated and analytic values. Thus, there is evidence that more Fourier components are needed in the basic transformation equations in order to handle cases of high triangular distortion.

9. SUMMARY

The Grad-Shafranov test criteria introduced here consist of formulae for the properties of a magnetically confined toroidal plasma, where these formulae are derived from the simplest set of analytic solutions to the Grad-Shafranov equation (a subset of the "Solov'ev solutions," Ref. 7). The plasma is assumed to be toroidally symmetric and to contain nested flux surfaces. To establish the framework, a flux-surface coordinate system (ρ,θ,ϕ) is described in which the principal coordinate ρ corresponds one-to-one with flux surfaces that are movable with respect to fixed cylindrical coordinates (R,Z,ϕ); R denotes the local major radius, Z the vertical displacement from the horizontal midplane, and ϕ the toroidal angle. Using these (ρ,θ,ϕ) coordinates, the source of the Grad-Shafranov equation is reviewed. This equation governs the 2-D distribution of poloidal magnetic flux $\chi(\rho)$ under quasistationary conditions. Tractable analytic solutions exist if the equation is made subject to the constraints:

$$\frac{2\pi c}{\chi(\rho,t)} \frac{\partial P(\rho,t)}{\partial \rho} \equiv -A_o \ , \tag{9.1}$$

and

$$\frac{c}{2} \frac{g(\rho,t)}{\chi(\rho,t)} \frac{\partial g(\rho,t)}{\partial \rho} \equiv 0 \ , \tag{9.2}$$

where $P(\rho,t)$ denotes plasma pressure, $\chi'(\rho,t) \equiv \partial\chi(\rho,t)/\partial\rho$ represents poloidal magnetic-flux density, and $g(\rho,t) \equiv R^2(\vec{B}\cdot\vec{\nabla}\phi)$ is the toroidal flux function. These constraints impose limitations on use of the test criteria derived from the analytic solutions. The latter can be parameterized with respect to the principal flux coordinate ρ and arranged into families of nested toroidal flux surfaces having similar shape patterns, where each family converges uniformly as $\rho \to 0$ onto a common circular loop of radius R_m (i.e., onto the "magnetic axis"). The analytic formulae for properties of a given family constitute the test criteria which include: (1) geometric properties associated with the flux surfaces; (2) the total toroidal current; (3) the plasma-pressure profile; and, (4) the poloidal flux density $\chi'(\rho,t)$ versus ρ.

As a first application of these test criteria, the performance of a 1-1/2-D extension to the BALDUR transport code has been checked. This code was assembled by linking a MHD-equilibrium subprogram to a version of BALDUR which had been upgraded to nonorthogonal flux coordinates (ρ,θ,ϕ). The MHD part is based on the Grad-Shafranov equation and determines as a function of time the 2-D flux-surface geometry as well as the poloidal current. The BALDUR part simulates, on a resistive time scale, the evolution and 1-D cross-field transport of flux-surface-averaged plasma properties; it also advances the poloidal flux-density profile and includes a model for ohmic heating which is more explicit than used before. Comparisons between code calculations and the test criteria were made more meaningful by introducing certain temporary modifications into the code. These involved algorithms which forced consistency with the analytic solutions through readjusting the following: (1) geometric triangularity; (2) total toroidal current; (3) the plasma-pressure profile; and (4) the variation of plasma resistivity with ρ. The last two were sufficient to ensure that the code calculations satisfied the

first analytic constraint (9.1). No changes were introduced to guarantee compliance with the second constraint (9.2) since it was not clear how to do this; instead, the departure of code calculations from the second constraint was always measured after the fact. In an attempt to optimize overall consistency, two methods were alternately employed for determining the toroidal current profile, $I(\rho)$ versus ρ. One was the method built into the code for general use (i.e., numerical solution of a nonlinear diffusion equation for poloidal flux density), the other involved a simple formula valid only for the special analytic solutions. The first turned out to be superior from the standpoint of overall consistency, and was always used thereafter. Typical results of code-calculated versus analytically determined values are set out for two cases: one displaying good agreement (i.e., Exhibit A and Table 1), the other poor (i.e., Exhibit B and Table 2). Departure from the second constraint is just one of the properties included in these comparisons (see Tables 1 and 2). The results show that the MHD subprogram is capable of representing cases of high ellipticity, but exhibits weakness in cases of appreciable triangular distortion D(a) as defined by

$$D(a) \equiv \left|R_o - \hat{R}(a)\right|/a \ , \tag{9.3}$$

where R_o denotes the major radius to the center of the outermost flux surface, "a" is the horizontal half-width ("minor radius") of this surface, and $\hat{R}(a)$ is the major radius to the point on this surface furthest above the horizontal midplane. Moreover, it was found that, when $D(a) > 0.4$, the MHD numerical model often failed to converge; and, this may have something to do with having only three Fourier components.

In the course of testing the BALDUR-VMOMS code, a parameter study was

made to determine the adjustments which yielded best agreement with analytic values. The prescribed variations included: (1) varying the finite-difference grid size with respect to both ρ and θ; (2) adjusting the minimum value of $x \equiv \rho/a$ (slightly above zero in order to avoid singularities); (3) changing the error limits imposed on internal iterations; (4) enhancing the level of plasma pressure, and hence the magnitude of $\partial P(\rho,t)/\partial\rho$ in (9.1); and, (5) multiplying the prescribed vacuum toroidal field by a factor of 2. Once a certain performance was reached, none of the above variations had any appreciable effect on reducing the differences between code-calculated and analytically determined values and, in particular, did not improve the case set out in Exhibit B and Table 2 (i.e., Case B). This behavior suggested that the source of the discrepancies was Fourier truncation. An alternative explanation involving the second constraint (9.2) was not able to account fully for the observed discrepancies (see Table 3). In another part of the parameter study, when the plasma pressure was increased by a factor of 100, the MHD model behaved as it should by scaling the following quantities precisely in agreement with basic physical principles: (1) the poloidal flux density $\chi(\rho,t)$, (2) the toroidal current profile, and (3) the gradient of poloidal current. Incidentally, the gradient of poloidal current vanishes in the case of the analytic solutions, due to imposing the second constraint [i.e., (9.2) implies that $J\cdot\nabla\theta = 0$, see (6.5) and (6.6)].

One of the most interesting results concerns the numerical calculation of poloidal flux density $\chi(\rho,t)$. In cases where the code-calculations nearly satisfied the second constraint (9.2) (e.g., see Table 1), agreement between code-calculated and analytically determined values of $\chi(\rho,t)$, over $0 < \rho \leq a$, turned out better than one part in 50,000, even under ellipticities of 2.0 (see Exhibit A). Of course, since plasma resistivity $\eta_{\parallel}$ was being prescribed

according to (8.18) or (7.41), the nonlinear effects in a more realistic representation of resistivity were not included. However, the results remain a significant test of the algorithm for calculating poloidal flux density.

As a final result of performance tests reported here, a partial list of suggested parameter values is set out below for the first MHD subprogram (i.e., Ref. 18) linked to the BALDUR transport code:

number of MHD spatial zones	20
number of poloidal-angle grid points	11
minimum value of x = a/a	0.02
error-limit criteria	ERROR =xerror=1.e-03
	PARERR=xparer=1.e-03

In view of weakness in the present code when handling cases of appreciable triangular distortion, work is under way on modifications which will allow a more accurate MHD treatment. However, it might be well to remember that this first MHD subprogram does offer appreciable computational efficiency. Typically, using 50 BALDUR grid points and 40 MHD zones (other settings as shown above), the VMOMS MHD subprogram (Ref. 18) when coupled to the BALDUR transport code requires ~0.5 second to converge on the CRAY-1 machines.

ACKNOWLEDGMENTS

The author wishes to express his gratitude to both D. E. Post and D. R. Mikkelsen of the Princeton Plasma Physics Laboratory (PPPL) who suggested making the attempt to link the 1-D BALDUR transport code with the VMOMS 2-D equilibrium code, and then to check the consequences. Moreover, it is a pleasure to thank G. Bateman (of PPPL) for his advice on certain aspects of this 1-1/2-D BALDUR-VMOMS linkage, particularly on preserving plasma properties with respect to toroidal flux. Considerable appreciation is also due M. Reusch (of PPPL) for allowing his unpublished notes (1983) to be used to check certain relations set out in Sec. 5. For the overall support of this investigation the author is very grateful to the U. S. Department of Energy Contract No. DE-AC02-76-CHO-3073.

REFERENCES

[1] C. E. Singer et al., "BALDUR: One-Dimensional Plasma Transport Code," Comput. Phys. Commun. (to be published).

[2] A. Silverman, D. E. Post, C. E. Singer, D. R. Mikkelsen, et al., "BALDUR: One-Dimensional Plasma Transport Code," Princeton Plasma Physics Laboratory, Applied Physics Division Report No. 23 (1983).

[3] D. Heifetz et al., "A Monte Carlo Model of Neutral Particle Transport in Diverted Plasmas," J. Comput. Phys. 46, 309 (1982).

[4] M. Petravic et al., "Cool, High-Density Regime for Poloidal Divertors," Phys. Rev. Lett. 48, 326 (1982).

[5] R. A. Hulse, "Numerical Studies of Impurities in Fusion Plasmas," Nucl. Technol./Fus. 3, 259 (1983).

[6] V. D. Shafranov, "Plasma Equilibrium in a Magnetic Field," Reviews of Plasma Physics, Vol. 2, edited by M. A. Leontovich, trans. by H. Lashinsky (Consultants Bureau, NY, 1966).

[7] L. S. Solov'ev, "The Theory of Hydromagnetic Stability of Toroidal Plasma Configurations," Sov. Phys. JETP 26, 400 (1968) trans. by D. ter Haar.

[8] F. Seidl, D. Post, D. Mikkelsen, and C. Boley, "Upgrade of the BALDUR Transport Code to Include Non-Circular Flux Surfaces," Bull. Am. Phys. Soc. 28, 1209 (1983).

[9] A. H. Boozer, "Evaluation of the Structure of Ergodic Fields," Phys. Fluids 26, 1288 (1983).

[10] M. D. Kruskal and R. M. Kulsrud, "Equilibrium of a Magnetically Confined Plasma in a Toroid," Phys. Fluids 1, 265 (1958).

[11] L. L. Lao, S. P. Hirshman, and R. M. Wieland, "Variational Moment Solutions to the Grad-Shafranov Equation," Phys. Fluids 24, 1431 (1981).

[12] S. P. Hirshman and S. C. Jardin, "Two-Dimensional Transport of Tokamak

Plasmas," Phys. Fluids 22, 731 (1979); S. C. Jardin, "Self-Consistent Solutions of the Plasma Transport Equations in an Axisymmetric Toroidal System," J. Comput. Phys. 43, 31 (1981).

[13] F. L. Hinton and R. D. Hazeltine, "Theory of Plasma Transport in Toroidal Confinement Systems," Rev. Mod. Phys. 48, 239 (1976).

[14] S. P. Hirshman and D. J. Sigmar, "Neoclassical Transport of Impurities in Tokamak Plasmas," Nucl. Fusion 21, 1079 (1981).

[15] S. L. Hirshman, "Neoclassical Current in a Toroidally-Confined Multispecies Plasma," Phys. Fluids 21, 1295 (1978).

[16] I. S. Gradshteyn, I. M. Ryzhik, Y. V. Geronimus, and M. Y. Tseytlin, "Table of Integral, Series, and Products;" trans. and edited by A. Jeffrey (Academic Press, NY, 1980).

[17] L. Spitzer, "Physics of Fully Ionized Gases," Interscience (second revision edition) (1967).

[18] L. L. Lao, R. M. Wieland, W. A. Houlberg, and S. P. Hirshman, "VMOMS - A Computer Code for Finding Moment Solutions to the Grad-Shafranov Equation," Comput. Phys. Commun. 27, 129 (1982).

1A EXHIBIT A ********** moments(external) ********** EXHIBIT A

i	r (cm)	p (ev/cm**3)	ai (amps)	shift (cm)	elong	triang	zshift	zelong	ztrang	zlamba	zvolmi
1	0.00	1.520e+18	0.	0.	2.000e+00	0.	0.	0.	0.	0.	0.
2	1.70	1.519e+18	1.485e+03	1.824e-04	2.000e+00	8.987e-05	2.898e-04	2.000e+00	1.700e-04	4.623e-07	5.705e+17
3	3.40	1.517e+18	5.940e+03	9.198e-04	2.000e+00	3.102e-04	1.156e-03	2.000e+00	3.400e-04	1.849e-06	2.282e+18
4	5.10	1.514e+18	1.336e+04	2.414e-03	2.000e+00	5.212e-04	2.601e-03	2.000e+00	5.099e-04	4.160e-06	5.135e+18
5	6.80	1.510e+18	2.376e+04	4.457e-03	2.000e+00	7.341e-04	4.623e-03	2.000e+00	6.799e-04	7.396e-06	9.128e+18
6	8.50	1.505e+18	3.712e+04	7.042e-03	2.000e+00	8.757e-04	7.224e-03	2.000e+00	8.499e-04	1.156e-05	1.426e+19
7	10.20	1.498e+18	5.346e+04	1.020e-02	2.000e+00	1.047e-03	1.040e-02	2.000e+00	1.020e-03	1.664e-05	2.054e+19
8	11.90	1.490e+18	7.276e+04	1.394e-02	2.000e+00	1.222e-03	1.416e-02	2.000e+00	1.190e-03	2.265e-05	2.796e+19
9	13.60	1.481e+18	9.503e+04	1.827e-02	2.000e+00	1.398e-03	1.849e-02	2.000e+00	1.360e-03	2.958e-05	3.651e+19
10	15.30	1.471e+18	1.203e+05	2.317e-02	2.000e+00	1.573e-03	2.341e-02	2.000e+00	1.530e-03	3.744e-05	4.621e+19
11	17.00	1.459e+18	1.485e+05	2.865e-02	2.000e+00	1.748e-03	2.894e-02	2.000e+00	1.700e-03	4.623e-05	5.705e+19
12	18.70	1.446e+18	1.797e+05	3.471e-02	2.000e+00	1.923e-03	3.496e-02	2.000e+00	1.870e-03	5.593e-05	6.903e+19
13	20.40	1.433e+18	2.138e+05	4.134e-02	2.000e+00	2.097e-03	4.161e-02	2.000e+00	2.040e-03	6.657e-05	8.215e+19
14	22.10	1.417e+18	2.509e+05	4.854e-02	2.000e+00	2.272e-03	4.883e-02	2.000e+00	2.210e-03	7.812e-05	9.642e+19
15	23.80	1.401e+18	2.910e+05	5.633e-02	2.000e+00	2.447e-03	5.664e-02	2.000e+00	2.380e-03	9.060e-05	1.118e+20
16	25.50	1.383e+18	3.341e+05	6.469e-02	2.000e+00	2.622e-03	6.502e-02	2.000e+00	2.550e-03	1.040e-04	1.284e+20
17	27.20	1.365e+18	3.801e+05	7.363e-02	2.000e+00	2.796e-03	7.397e-02	2.000e+00	2.720e-03	1.183e-04	1.461e+20
18	28.90	1.345e+18	4.291e+05	8.314e-02	2.000e+00	2.971e-03	8.351e-02	2.000e+00	2.890e-03	1.336e-04	1.649e+20
19	30.60	1.323e+18	4.811e+05	9.323e-02	2.000e+00	3.146e-03	9.362e-02	2.000e+00	3.060e-03	1.498e-04	1.848e+20
20	32.30	1.301e+18	5.360e+05	1.039e-01	2.000e+00	3.321e-03	1.043e-01	2.000e+00	3.230e-03	1.669e-04	2.060e+20
21	34.00	1.277e+18	5.939e+05	1.151e-01	2.000e+00	3.496e-03	1.156e-01	2.000e+00	3.400e-03	1.849e-04	2.282e+20
22	35.70	1.252e+18	6.548e+05	1.270e-01	2.000e+00	3.671e-03	1.274e-01	2.000e+00	3.570e-03	2.038e-04	2.516e+20
23	37.40	1.226e+18	7.186e+05	1.394e-01	2.000e+00	3.846e-03	1.399e-01	2.000e+00	3.740e-03	2.237e-04	2.761e+20
24	39.10	1.199e+18	7.855e+05	1.523e-01	2.000e+00	4.020e-03	1.529e-01	2.000e+00	3.910e-03	2.445e-04	3.018e+20
25	40.80	1.171e+18	8.552e+05	1.658e-01	2.000e+00	4.195e-03	1.664e-01	2.000e+00	4.080e-03	2.662e-04	3.286e+20
26	42.50	1.141e+18	9.280e+05	1.800e-01	2.000e+00	4.370e-03	1.806e-01	2.000e+00	4.250e-03	2.889e-04	3.566e+20
27	44.20	1.110e+18	1.004e+06	1.947e-01	2.000e+00	4.544e-03	1.953e-01	2.000e+00	4.420e-03	3.125e-04	3.857e+20
28	45.90	1.078e+18	1.082e+06	2.100e-01	2.000e+00	4.719e-03	2.107e-01	2.000e+00	4.590e-03	3.370e-04	4.159e+20
29	47.60	1.045e+18	1.164e+06	2.259e-01	2.000e+00	4.894e-03	2.266e-01	2.000e+00	4.760e-03	3.624e-04	4.473e+20
30	49.30	1.010e+18	1.249e+06	2.423e-01	2.000e+00	5.069e-03	2.430e-01	2.000e+00	4.930e-03	3.887e-04	4.798e+20
31	51.00	9.743e+17	1.336e+06	2.593e-01	2.000e+00	5.244e-03	2.601e-01	2.000e+00	5.100e-03	4.160e-04	5.134e+20
32	52.70	9.373e+17	1.427e+06	2.769e-01	2.000e+00	5.418e-03	2.777e-01	2.000e+00	5.270e-03	4.442e-04	5.482e+20
33	54.40	8.991e+17	1.520e+06	2.951e-01	2.000e+00	5.593e-03	2.959e-01	2.000e+00	5.440e-03	4.733e-04	5.842e+20
34	56.10	8.597e+17	1.617e+06	3.138e-01	2.000e+00	5.768e-03	3.147e-01	2.000e+00	5.610e-03	5.033e-04	6.213e+20
35	57.80	8.191e+17	1.716e+06	3.331e-01	2.000e+00	5.943e-03	3.340e-01	2.000e+00	5.780e-03	5.343e-04	6.595e+20
36	59.50	7.773e+17	1.819e+06	3.530e-01	2.000e+00	6.118e-03	3.540e-01	2.000e+00	5.950e-03	5.662e-04	6.988e+20
37	61.20	7.342e+17	1.924e+06	3.735e-01	2.000e+00	6.293e-03	3.745e-01	2.000e+00	6.120e-03	5.990e-04	7.393e+20
38	62.90	6.900e+17	2.033e+06	3.945e-01	2.000e+00	6.467e-03	3.956e-01	2.000e+00	6.290e-03	6.327e-04	7.810e+20
39	64.60	6.445e+17	2.144e+06	4.162e-01	2.000e+00	6.642e-03	4.173e-01	2.000e+00	6.460e-03	6.674e-04	8.238e+20
40	66.30	5.979e+17	2.258e+06	4.384e-01	2.000e+00	6.817e-03	4.395e-01	2.000e+00	6.630e-03	7.030e-04	8.677e+20
41	68.00	5.500e+17	2.375e+06	4.611e-01	2.000e+00	6.992e-03	4.624e-01	2.000e+00	6.800e-03	7.395e-04	9.127e+20
42	69.70	5.009e+17	2.496e+06	4.845e-01	2.000e+00	7.168e-03	4.858e-01	2.000e+00	6.970e-03	7.769e-04	9.590e+20
43	71.40	4.506e+17	2.619e+06	5.084e-01	2.000e+00	7.342e-03	5.097e-01	2.000e+00	7.140e-03	8.153e-04	1.006e+21
44	73.10	3.991e+17	2.745e+06	5.330e-01	2.000e+00	7.514e-03	5.343e-01	2.000e+00	7.310e-03	8.546e-04	1.055e+21
45	74.80	3.464e+17	2.874e+06	5.581e-01	2.000e+00	7.687e-03	5.595e-01	2.000e+00	7.480e-03	8.947e-04	1.104e+21
46	76.50	2.924e+17	3.006e+06	5.837e-01	2.000e+00	7.860e-03	5.852e-01	2.000e+00	7.650e-03	9.359e-04	1.155e+21
47	78.20	2.373e+17	3.141e+06	6.099e-01	2.000e+00	8.033e-03	6.115e-01	2.000e+00	7.820e-03	9.779e-04	1.207e+21
48	79.90	1.809e+17	3.279e+06	6.367e-01	2.000e+00	8.224e-03	6.383e-01	2.000e+00	7.990e-03	1.021e-03	1.260e+21
49	81.60	1.234e+17	3.420e+06	6.643e-01	2.000e+00	8.365e-03	6.658e-01	2.000e+00	8.160e-03	1.065e-03	1.314e+21
50	83.30	6.460e+16	3.564e+06	6.928e-01	2.000e+00	8.461e-03	6.938e-01	2.000e+00	8.331e-03	1.110e-03	1.370e+21
51	85.00	4.615e+15	3.711e+06	7.224e-01	2.000e+00	8.501e-03	7.224e-01	2.000e+00	8.501e-03	1.155e-03	1.426e+21

2A EXHIBIT A comparisons of normalized poloidal magnetic flux densities (internal units).

EXHIBIT A

"bpoli(j)" results from using the baldur-mhd code
"zbpoli(j)" is obtained from an analytic formula

i	r	zradjs	zelong	zbpoli	ybpoli	bpoli	beta-pol
1	0.00	5.0007e+03	0.	0.	0.	0.	1.0000e+34
2	1.70	5.0007e+03	2.0000e+00	1.3977e+01	1.3976e+01	1.3977e+01	5.2700e+03
3	3.40	5.0007e+03	2.0000e+00	2.7953e+01	2.7953e+01	2.7954e+01	1.3159e+03
4	5.10	5.0007e+03	2.0000e+00	4.1930e+01	4.1929e+01	4.1931e+01	5.8369e+02
5	6.80	5.0007e+03	2.0000e+00	5.5907e+01	5.5906e+01	5.5908e+01	3.2741e+02
6	8.50	5.0007e+03	2.0000e+00	6.9883e+01	6.9882e+01	6.9885e+01	2.0878e+02
7	10.20	5.0007e+03	2.0000e+00	8.3860e+01	8.3858e+01	8.3862e+01	1.4436e+02
8	11.90	5.0007e+03	2.0000e+00	9.7836e+01	9.7834e+01	9.7838e+01	1.0549e+02
9	13.60	5.0007e+03	2.0000e+00	1.1181e+02	1.1181e+02	1.1181e+02	8.0275e+01
10	15.30	5.0007e+03	2.0000e+00	1.2579e+02	1.2579e+02	1.2579e+02	6.2986e+01
11	17.00	5.0007e+03	2.0000e+00	1.3976e+02	1.3976e+02	1.3977e+02	5.0619e+01
12	18.70	5.0007e+03	2.0000e+00	1.5374e+02	1.5374e+02	1.5374e+02	4.1470e+01
13	20.40	5.0007e+03	2.0000e+00	1.6771e+02	1.6771e+02	1.6772e+02	3.4510e+01
14	22.10	5.0007e+03	2.0000e+00	1.8169e+02	1.8169e+02	1.8169e+02	2.9094e+01
15	23.80	5.0007e+03	2.0000e+00	1.9567e+02	1.9566e+02	1.9567e+02	2.4797e+01
16	25.50	5.0007e+03	2.0000e+00	2.0964e+02	2.0964e+02	2.0964e+02	2.1330e+01
17	27.20	5.0006e+03	2.0000e+00	2.2361e+02	2.2361e+02	2.2362e+02	1.8492e+01
18	28.90	5.0006e+03	2.0000e+00	2.3759e+02	2.3758e+02	2.3759e+02	1.6141e+01
19	30.60	5.0006e+03	2.0000e+00	2.5156e+02	2.5156e+02	2.5157e+02	1.4170e+01
20	32.30	5.0006e+03	2.0000e+00	2.6554e+02	2.6553e+02	2.6554e+02	1.2502e+01
21	34.00	5.0006e+03	2.0000e+00	2.7951e+02	2.7950e+02	2.7951e+02	1.1078e+01
22	35.70	5.0006e+03	2.0000e+00	2.9348e+02	2.9348e+02	2.9349e+02	9.8530e+00
23	37.40	5.0006e+03	2.0000e+00	3.0745e+02	3.0745e+02	3.0746e+02	8.7909e+00
24	39.10	5.0006e+03	2.0000e+00	3.2142e+02	3.2142e+02	3.2143e+02	7.8643e+00
25	40.80	5.0006e+03	2.0000e+00	3.3540e+02	3.3539e+02	3.3540e+02	7.0511e+00
26	42.50	5.0005e+03	2.0000e+00	3.4937e+02	3.4936e+02	3.4937e+02	6.3335e+00
27	44.20	5.0005e+03	2.0000e+00	3.6334e+02	3.6333e+02	3.6334e+02	5.6971e+00
28	45.90	5.0005e+03	2.0000e+00	3.7731e+02	3.7730e+02	3.7731e+02	5.1300e+00
29	47.60	5.0005e+03	2.0000e+00	3.9128e+02	3.9127e+02	3.9128e+02	4.6227e+00
30	49.30	5.0005e+03	2.0000e+00	4.0525e+02	4.0524e+02	4.0525e+02	4.1669e+00
31	51.00	5.0005e+03	2.0000e+00	4.1921e+02	4.1921e+02	4.1922e+02	3.7559e+00
32	52.70	5.0004e+03	2.0000e+00	4.3318e+02	4.3318e+02	4.3318e+02	3.3841e+00
33	54.40	5.0004e+03	2.0000e+00	4.4715e+02	4.4714e+02	4.4715e+02	3.0465e+00
34	56.10	5.0004e+03	2.0000e+00	4.6112e+02	4.6111e+02	4.6111e+02	2.7392e+00
35	57.80	5.0004e+03	2.0000e+00	4.7508e+02	4.7508e+02	4.7508e+02	2.4586e+00
36	59.50	5.0004e+03	2.0000e+00	4.8905e+02	4.8904e+02	4.8904e+02	2.2017e+00
37	61.20	5.0003e+03	2.0000e+00	5.0301e+02	5.0301e+02	5.0301e+02	1.9659e+00
38	62.90	5.0003e+03	2.0000e+00	5.1697e+02	5.1697e+02	5.1697e+02	1.7489e+00
39	64.60	5.0003e+03	2.0000e+00	5.3094e+02	5.3093e+02	5.3093e+02	1.5489e+00
40	66.30	5.0003e+03	2.0000e+00	5.4490e+02	5.4490e+02	5.4489e+02	1.3648e+00
41	68.00	5.0003e+03	2.0000e+00	5.5886e+02	5.5886e+02	5.5885e+02	1.1929e+00
42	69.70	5.0002e+03	2.0000e+00	5.7282e+02	5.7282e+02	5.7281e+02	1.0341e+00
43	71.40	5.0002e+03	2.0000e+00	5.8678e+02	5.8678e+02	5.8677e+02	8.8649e-01
44	73.10	5.0002e+03	2.0000e+00	6.0074e+02	6.0074e+02	6.0073e+02	7.4987e-01
45	74.80	5.0002e+03	2.0000e+00	6.1470e+02	6.1470e+02	6.1469e+02	6.2092e-01
46	76.50	5.0001e+03	2.0000e+00	6.2866e+02	6.2865e+02	6.2864e+02	5.0120e-01
47	78.20	5.0001e+03	2.0000e+00	6.4261e+02	6.4261e+02	6.4260e+02	3.8921e-01
48	79.90	5.0001e+03	2.0000e+00	6.5657e+02	6.5657e+02	6.5655e+02	2.8429e-01
49	81.60	5.0001e+03	2.0000e+00	6.7052e+02	6.7052e+02	6.7050e+02	1.8506e-01
50	83.30	5.0000e+03	2.0000e+00	6.8448e+02	6.8448e+02	6.8445e+02	9.3380e-02

i	r (cm)	p (ev/cm**3)	ai (amps)	shift (cm)	elong	triang	zshift	zelong	ztrang	zlamba	zvolmi
1	0.00	1.528e+18	0.	0.	1.511e+00	0.	0.	0.	0.	0.	0.
2	1.70	1.519e+18	1.416e+03	2.822e-03	1.511e+00	3.582e-03	8.823e-03	1.000e+00	5.190e-03	4.309e-04	1.484e+16
3	3.40	1.517e+18	5.662e+03	2.684e-02	1.511e+00	1.167e-02	3.529e-02	1.000e+00	1.038e-02	1.723e-03	5.617e+16
4	5.10	1.512e+18	1.273e+04	7.079e-02	1.512e+00	1.951e-02	7.942e-02	1.000e+00	1.558e-02	3.875e-03	1.264e+17
5	6.80	1.507e+18	2.264e+04	1.310e-01	1.512e+00	2.633e-02	1.412e-01	1.000e+00	2.079e-02	6.883e-03	2.246e+17
6	8.50	1.499e+18	3.535e+04	2.073e-01	1.512e+00	3.274e-02	2.207e-01	1.000e+00	2.600e-02	1.074e-02	3.507e+17
7	10.20	1.490e+18	5.086e+04	3.004e-01	1.512e+00	3.917e-02	3.179e-01	1.000e+00	3.123e-02	1.545e-02	5.047e+17
8	11.90	1.479e+18	6.921e+04	4.110e-01	1.513e+00	4.578e-02	4.329e-01	1.000e+00	3.647e-02	2.100e-02	6.864e+17
9	13.60	1.467e+18	9.027e+04	5.398e-01	1.513e+00	5.228e-02	5.656e-01	1.000e+00	4.173e-02	2.739e-02	8.958e+17
10	15.30	1.453e+18	1.142e+05	6.841e-01	1.514e+00	5.886e-02	7.162e-01	1.000e+00	4.702e-02	3.460e-02	1.133e+18
11	17.00	1.438e+18	1.408e+05	8.463e-01	1.515e+00	6.543e-02	8.847e-01	1.000e+00	5.232e-02	4.263e-02	1.397e+18
12	18.70	1.421e+18	1.701e+05	1.026e+00	1.516e+00	7.201e-02	1.071e+00	1.000e+00	5.765e-02	5.146e-02	1.688e+18
13	20.40	1.402e+18	2.023e+05	1.223e+00	1.516e+00	7.860e-02	1.275e+00	1.000e+00	6.302e-02	6.109e-02	2.007e+18
14	22.10	1.382e+18	2.371e+05	1.437e+00	1.517e+00	8.528e-02	1.498e+00	1.000e+00	6.841e-02	7.150e-02	2.352e+18
15	23.80	1.361e+18	2.745e+05	1.669e+00	1.518e+00	9.182e-02	1.738e+00	1.000e+00	7.384e-02	8.268e-02	2.723e+18
16	25.50	1.338e+18	3.147e+05	1.918e+00	1.520e+00	9.845e-02	1.997e+00	1.000e+00	7.930e-02	9.461e-02	3.121e+18
17	27.20	1.313e+18	3.572e+05	2.185e+00	1.521e+00	1.051e-01	2.274e+00	1.000e+00	8.481e-02	1.073e-01	3.544e+18
18	28.90	1.288e+18	4.028e+05	2.470e+00	1.522e+00	1.118e-01	2.570e+00	1.000e+00	9.036e-02	1.207e-01	3.994e+18
19	30.60	1.260e+18	4.506e+05	2.772e+00	1.523e+00	1.184e-01	2.884e+00	1.000e+00	9.597e-02	1.348e-01	4.468e+18
20	32.30	1.232e+18	5.008e+05	3.093e+00	1.525e+00	1.251e-01	3.217e+00	1.000e+00	1.016e-01	1.495e-01	4.968e+18
21	34.00	1.202e+18	5.540e+05	3.431e+00	1.526e+00	1.318e-01	3.568e+00	1.000e+00	1.073e-01	1.649e-01	5.492e+18
22	35.70	1.171e+18	6.098e+05	3.788e+00	1.528e+00	1.386e-01	3.938e+00	1.000e+00	1.131e-01	1.810e-01	6.040e+18
23	37.40	1.139e+18	6.678e+05	4.163e+00	1.529e+00	1.453e-01	4.327e+00	1.000e+00	1.189e-01	1.977e-01	6.612e+18
24	39.10	1.106e+18	7.271e+05	4.557e+00	1.531e+00	1.521e-01	4.736e+00	1.000e+00	1.248e-01	2.150e-01	7.207e+18
25	40.80	1.072e+18	7.888e+05	4.969e+00	1.533e+00	1.589e-01	5.163e+00	1.000e+00	1.308e-01	2.328e-01	7.825e+18
26	42.50	1.036e+18	8.543e+05	5.400e+00	1.535e+00	1.657e-01	5.610e+00	1.000e+00	1.369e-01	2.512e-01	8.465e+18
27	44.20	9.999e+17	9.209e+05	5.850e+00	1.537e+00	1.725e-01	6.077e+00	1.000e+00	1.430e-01	2.701e-01	9.126e+18
28	45.90	9.626e+17	9.898e+05	6.320e+00	1.539e+00	1.794e-01	6.563e+00	1.000e+00	1.492e-01	2.895e-01	9.809e+18
29	47.60	9.244e+17	1.061e+06	6.808e+00	1.541e+00	1.863e-01	7.070e+00	1.000e+00	1.555e-01	3.093e-01	1.051e+19
30	49.30	8.854e+17	1.134e+06	7.316e+00	1.543e+00	1.932e-01	7.596e+00	1.000e+00	1.620e-01	3.296e-01	1.124e+19
31	51.00	8.457e+17	1.209e+06	7.844e+00	1.546e+00	2.001e-01	8.143e+00	1.000e+00	1.685e-01	3.502e-01	1.198e+19
32	52.70	8.052e+17	1.286e+06	8.392e+00	1.548e+00	2.070e-01	8.710e+00	1.000e+00	1.751e-01	3.713e-01	1.274e+19
33	54.40	7.641e+17	1.365e+06	8.960e+00	1.550e+00	2.139e-01	9.298e+00	1.000e+00	1.819e-01	3.926e-01	1.352e+19
34	56.10	7.225e+17	1.446e+06	9.548e+00	1.553e+00	2.209e-01	9.908e+00	1.000e+00	1.888e-01	4.142e-01	1.431e+19
35	57.80	6.804e+17	1.527e+06	1.016e+01	1.555e+00	2.279e-01	1.054e+01	1.000e+00	1.958e-01	4.361e-01	1.512e+19
36	59.50	6.378e+17	1.612e+06	1.079e+01	1.558e+00	2.349e-01	1.119e+01	1.000e+00	2.030e-01	4.582e-01	1.595e+19
37	61.20	5.949e+17	1.697e+06	1.144e+01	1.561e+00	2.419e-01	1.186e+01	1.000e+00	2.103e-01	4.805e-01	1.679e+19
38	62.90	5.517e+17	1.782e+06	1.211e+01	1.563e+00	2.489e-01	1.256e+01	1.000e+00	2.178e-01	5.029e-01	1.764e+19
39	64.60	5.084e+17	1.872e+06	1.281e+01	1.566e+00	2.559e-01	1.328e+01	1.000e+00	2.255e-01	5.255e-01	1.850e+19
40	66.30	4.649e+17	1.968e+06	1.352e+01	1.569e+00	2.630e-01	1.402e+01	1.000e+00	2.334e-01	5.481e-01	1.938e+19
41	68.00	4.214e+17	2.050e+06	1.426e+01	1.572e+00	2.700e-01	1.478e+01	1.000e+00	2.415e-01	5.707e-01	2.026e+19
42	69.70	3.780e+17	2.142e+06	1.503e+01	1.575e+00	2.770e-01	1.557e+01	1.000e+00	2.498e-01	5.932e-01	2.116e+19
43	71.40	3.347e+17	2.232e+06	1.581e+01	1.578e+00	2.840e-01	1.638e+01	1.000e+00	2.584e-01	6.157e-01	2.206e+19
44	73.10	2.916e+17	2.326e+06	1.662e+01	1.581e+00	2.910e-01	1.722e+01	1.000e+00	2.672e-01	6.381e-01	2.296e+19
45	74.80	2.489e+17	2.419e+06	1.746e+01	1.584e+00	2.979e-01	1.808e+01	1.000e+00	2.763e-01	6.603e-01	2.387e+19
46	76.50	2.065e+17	2.511e+06	1.832e+01	1.587e+00	3.048e-01	1.896e+01	1.000e+00	2.857e-01	6.823e-01	2.478e+19
47	78.20	1.647e+17	2.605e+06	1.920e+01	1.590e+00	3.117e-01	1.987e+01	1.000e+00	2.954e-01	7.040e-01	2.569e+19
48	79.90	1.235e+17	2.699e+06	2.011e+01	1.592e+00	3.185e-01	2.081e+01	1.000e+00	3.055e-01	7.254e-01	2.660e+19
49	81.60	8.385e+16	2.792e+06	2.104e+01	1.595e+00	3.252e-01	2.177e+01	1.000e+00	3.160e-01	7.464e-01	2.751e+19
50	83.30	4.338e+16	2.886e+06	2.201e+01	1.598e+00	3.318e-01	2.277e+01	1.000e+00	3.269e-01	7.670e-01	2.841e+19
51	85.00	4.615e+15	2.980e+06	2.302e+01	1.600e+00	3.383e-01	2.378e+01	1.000e+00	3.383e-01	7.872e-01	2.930e+19

EXHIBIT B

comparisons of normalized poloidal magnetic flux densities (internal units).

"bpoli(j)" results from using the baldur-mhd code
"zbpoli (j)" is obtained from an analytic formula

i	r	zradjs	zelong	zbpoli	ybpoli	bpoli
1	0.00	1.6378e+02	0.	0.	0.	0.
2	1.70	1.6377e+02	1.6000e+00	1.8128e+01	1.7342e+01	1.7837e+01
3	3.40	1.6375e+02	1.6000e+00	3.6230e+01	3.4664e+01	3.5647e+01
4	5.10	1.6370e+02	1.6000e+00	5.4286e+01	5.1994e+01	5.3417e+01
5	6.80	1.6364e+02	1.6000e+00	7.2272e+01	6.9167e+01	7.1137e+01
6	8.50	1.6356e+02	1.6000e+00	9.0165e+01	8.6389e+01	8.8742e+01
7	10.20	1.6347e+02	1.6000e+00	1.0794e+02	1.0336e+02	1.0625e+02
8	11.90	1.6335e+02	1.6000e+00	1.2557e+02	1.2019e+02	1.2362e+02
9	13.60	1.6322e+02	1.6000e+00	1.4304e+02	1.3700e+02	1.4082e+02
10	15.30	1.6307e+02	1.6000e+00	1.6033e+02	1.5351e+02	1.5787e+02
11	17.00	1.6290e+02	1.6000e+00	1.7748e+02	1.6987e+02	1.7470e+02
12	18.70	1.6271e+02	1.6000e+00	1.9424e+02	1.8614e+02	1.9130e+02
13	20.40	1.6251e+02	1.6000e+00	2.1082e+02	2.0191e+02	2.0769e+02
14	22.10	1.6229e+02	1.6000e+00	2.2712e+02	2.1760e+02	2.2376e+02
15	23.80	1.6204e+02	1.6000e+00	2.4311e+02	2.3296e+02	2.3956e+02
16	25.50	1.6179e+02	1.6000e+00	2.5877e+02	2.4794e+02	2.5506e+02
17	27.20	1.6151e+02	1.6000e+00	2.7409e+02	2.6285e+02	2.7019e+02
18	28.90	1.6121e+02	1.6000e+00	2.8903e+02	2.7704e+02	2.8501e+02
19	30.60	1.6090e+02	1.6000e+00	3.0357e+02	2.9106e+02	2.9941e+02
20	32.30	1.6057e+02	1.6000e+00	3.1769e+02	3.0476e+02	3.1340e+02
21	34.00	1.6022e+02	1.6000e+00	3.3136e+02	3.1775e+02	3.2699e+02
22	35.70	1.5985e+02	1.6000e+00	3.4456e+02	3.3066e+02	3.4010e+02
23	37.40	1.5946e+02	1.6000e+00	3.5728e+02	3.4282e+02	3.5276e+02
24	39.10	1.5905e+02	1.6000e+00	3.6947e+02	3.5457e+02	3.6491e+02
25	40.80	1.5862e+02	1.6000e+00	3.8113e+02	3.6617e+02	3.7656e+02
26	42.50	1.5817e+02	1.6000e+00	3.9222e+02	3.7656e+02	3.8764e+02
27	44.20	1.5771e+02	1.6000e+00	4.0273e+02	3.8685e+02	3.9817e+02
28	45.90	1.5722e+02	1.6000e+00	4.1263e+02	3.9648e+02	4.0810e+02
29	47.60	1.5671e+02	1.6000e+00	4.2190e+02	4.0530e+02	4.1740e+02
30	49.30	1.5619e+02	1.6000e+00	4.3051e+02	4.1407e+02	4.2614e+02
31	51.00	1.5564e+02	1.6000e+00	4.3844e+02	4.2144e+02	4.3410e+02
32	52.70	1.5507e+02	1.6000e+00	4.4567e+02	4.2854e+02	4.4146e+02
33	54.40	1.5449e+02	1.6000e+00	4.5217e+02	4.3518e+02	4.4815e+02
34	56.10	1.5388e+02	1.6000e+00	4.5792e+02	4.4042e+02	4.5396e+02
35	57.80	1.5325e+02	1.6000e+00	4.6298e+02	4.4568e+02	4.5922e+02
36	59.50	1.5259e+02	1.6000e+00	4.6708e+02	4.4961e+02	4.6348e+02
37	61.20	1.5192e+02	1.6000e+00	4.7044e+02	4.5284e+02	4.6696e+02
38	62.90	1.5122e+02	1.6000e+00	4.7295e+02	4.5608e+02	4.6994e+02
39	64.60	1.5051e+02	1.6000e+00	4.7468e+02	4.5704e+02	4.7153e+02
40	66.30	1.4976e+02	1.6000e+00	4.7536e+02	4.5816e+02	4.7273e+02
41	68.00	1.4900e+02	1.6000e+00	4.7520e+02	4.5822e+02	4.7287e+02
42	69.70	1.4821e+02	1.6000e+00	4.7411e+02	4.5688e+02	4.7180e+02
43	71.40	1.4740e+02	1.6000e+00	4.7205e+02	4.5579e+02	4.7052e+02
44	73.10	1.4657e+02	1.6000e+00	4.6901e+02	4.5229e+02	4.6726e+02
45	74.80	1.4571e+02	1.6000e+00	4.6497e+02	4.4861e+02	4.6364e+02
46	76.50	1.4482e+02	1.6000e+00	4.5989e+02	4.4440e+02	4.5937e+02
47	78.20	1.4391e+02	1.6000e+00	4.5375e+02	4.3786e+02	4.5290e+02
48	79.90	1.4297e+02	1.6000e+00	4.4654e+02	4.3102e+02	4.4685e+02
49	81.60	1.4201e+02	1.6000e+00	4.3823e+02	4.2363e+02	4.3859e+02
50	83.30	1.4102e+02	1.6000e+00	4.2879e+02	4.1454e+02	4.2957e+02

TABLE 1

Departure of Numerical Results from the Second Analytic Constraint; i.e. from $B(\chi) \equiv 0$ [see Eq. (4.12)]. Run number=chkmhd22, R_o = 5000 cm, a = 85 cm, E(a)=2.0 [see Eq. (5.16)].

Radial Index i	Horiz. Minor Radius ρ(cm)	Max. Major Radius R_2(cm)	Min. Major Radius R_1(cm)	Cntral Major Radius R_G(cm)	Tri-angu-larity D(ρ)*	$A(\chi)R_G^2$ Eq.(6.1) × $\chi(\rho)$	$B(\chi)$ Eq.(6.2) × $\chi(\rho)$	$\lvert\epsilon(\chi)\rvert$ Eq.(8.30)
2	1.70	5002.4	4999.0	5000.7	0.0001	5.38(+21)	-3.72(+17)	6.91(-5)
9	13.60	5014.3	4987.1	5000.7	0.0014	4.31(+22)	-3.74(+18)	8.68(-5)
19	30.60	5031.2	4970.0	5000.6	0.0031	9.69(+22)	-6.27(+18)	6.47(-5)
29	47.60	5048.1	4952.9	5000.5	0.0049	1.51(+23)	-4.71(+18)	3.13(-5)
39	64.60	5064.9	4935.7	5000.3	0.0066	2.04(+23)	+5.50(+18)	2.69(-5)
49	81.60	5081.7	4918.5	5000.1	0.0084	2.58(+23)	+3.06(+19)	1.19(-4)

*From MHD Subprogram

TABLE 2

Departure of Numerical Results from the Second Analytic Constraint; i.e., from $B(\chi) \equiv 0$ [see Eq. (4.12)]. Run num.=tfmh33, R_o = 140cm, a = 85cm, E(a) = 1.6 [see Eq. (5.16)].

Radial Index i	Horiz. Minor Radius ρ(cm)	Max. Major Radius R_2(cm)	Min. Major Radius R_1(cm)	Cntral Major Radius R_G(cm)	Tri-angu-larity D(ρ)*	$A(\chi)R_G^2$ Eq.(6.1) × $\chi'(\rho)$	$B(\chi)$ Eq.(6.2) × $\chi'(\rho)$	$\lvert\varepsilon(\chi)\rvert$ Eq.(8.30)
2	1.70	165.47	162.07	163.77	0.0036	7.90(+18)	-7.43(+16)	0.94(-2)
9	13.60	176.82	149.62	163.22	0.0523	6.19(+19)	-7.84(+17)	1.27(-2)
19	30.60	191.50	130.30	160.90	0.1184	1.28(+20)	-1.74(+18)	1.36(-2)
29	47.60	204.31	109.11	156.71	0.1863	1.68(+20)	-3.20(+18)	1.90(-2)
39	64.60	215.11	85.91	150.51	0.2559	1.75(+20)	-3.36(+18)	1.93(-2)
49	81.60	223.61	60.41	142.01	0.3252	1.43(+20)	-3.70(+18)	2.58(-2)

*Obtained from MHD subprogram.

TABLE 3

Observed versus explainable discrepancies in Shafranov shift. Major Radius $\equiv R_o$ = 140 cm; radius to magnetic axis $\equiv R_m$ = 163.783...cm; Minor radius $\equiv$ a = 85 cm; elongation $\equiv$ E(a) = 1.60; triangularity $\equiv$ D(a) = 0.338.

(1) i	(2) ρ(cm)	(3) $(\frac{\Delta S}{S})_X$ Eq.(8.44)	(4) $\frac{R_o^2}{R_m R_G(\rho)}$	(5) $\bar{\varepsilon}(\rho)$ Eq.(8.51)	(6) $\hat{\varepsilon}(\rho)$ Eq.(8.52)	(7) $(\frac{\delta S}{S})_{\bar{\varepsilon}}$ Eq.(8.54)	(8) $(\frac{\delta S}{S})_{\hat{\varepsilon}}$ Eq.(8.55)
10	15.30	-0.0455	0.7339	-0.01335	-0.01626	-0.00980	-0.01193
20	32.30	-0.0392	0.7453	-0.01378	-0.02159	-0.01027	-0.01609
30	49.30	-0.0371	0.7662	-0.01883	-0.04020	-0.01443	-0.03080
40	66.30	-0.0357	0.7991	-0.01770	-0.05699	-0.01414	-0.04554
50	83.30	-0.0334	0.8486	-0.02764	-0.16499	-0.02346	-0.14001
51	a=85.00	-0.0328	0.8548	-----	-----	-----	-----

FIGURE CAPTIONS

FIG. 1. The geometric nature of the flux coordinate system employed here.

FIG. 2. Use of geometric elongation $E(\rho)$ and geometric triangularity $D(\rho)$ as measures of departure from circular symmetry, where $E(\rho) = b/\rho$ and $D(\rho) = \delta/\rho$; see Eqs. (5.16) and (5.17).

#86P0015

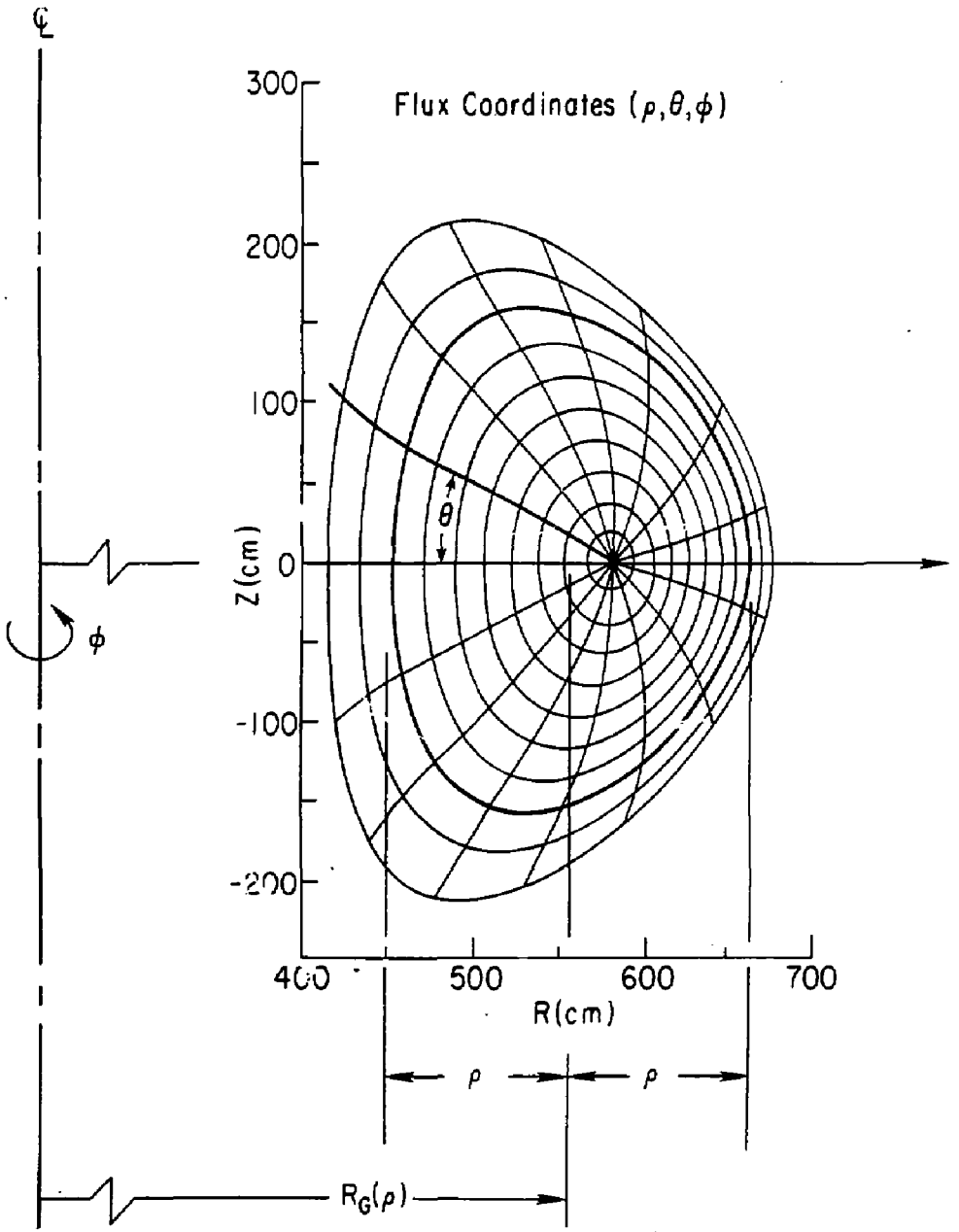

Fig. 1

#86P0014

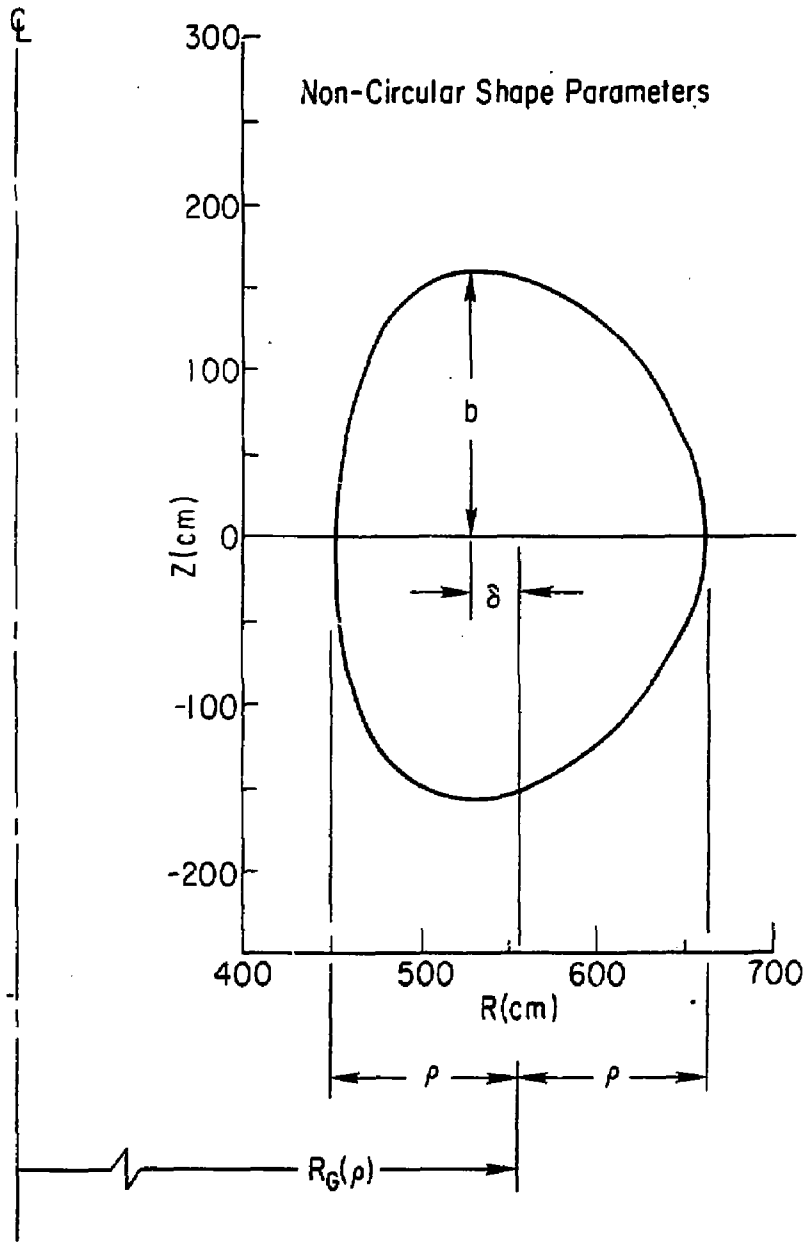

Fig. 2